

OSTRACODS FROM THE END-PERMIAN MASS EXTINCTION IN THE ARAS VALLEY SECTION (NORTH-WEST IRAN)

by JANA GLIWA¹ , MARIE-BÉATRICE FOREL² , SYLVIE CRASQUIN² ,
ABBAS GHADERI³  and DIETER KORN¹ 

¹Museum für Naturkunde, Leibniz Institute for Evolution & Biodiversity Science, Invalidenstraße 43, 10115, Berlin, Germany; jana.gliwa@mfn.berlin

²CR2P, MNHN-SU-CNRS, 8 rue Buffon, 75005, Paris, France

³Department of Geology, Faculty of Science, Ferdowsi University of Mashhad, Mashhad, Iran

Typescript received 13 December 2019; accepted in revised form 19 May 2020

Abstract: The Aras Valley section (north-west Iran) exposes a sedimentary succession that allows the study of ostracod diversity patterns during/across the end-Permian mass extinction. For the present study, 59 samples were investigated for their ostracod abundances, which ranged from 4 to 31 500 specimens per 500 g. In 45 sample horizons, the ostracods were identified to the species level. In total, 3 425 specimens were determined and 62 species were identified, of which one genus and ten species are described for the first time: *Fabalitypris veronicae* Gliwa, sp. nov., *Orthobairdia capuliformis* Gliwa, sp. nov., *Araxobairdia formosa* Gliwa, gen. et sp. nov., *Bairdiacypris kathleenae* Gliwa, sp. nov., *Eumiraculum mettei* Gliwa, sp. nov., *Liuzhinia julfensis* Gliwa, sp. nov., *Carinaknightina hofmanni* Gliwa, sp. nov., *Cavellina fosteri* Gliwa, sp. nov., *Cavellina hairapetiani* Gliwa, sp. nov. and *Hungaroleberis striatus* Forel, sp. nov.

The assemblages show, at the end-Permian mass extinction event, a complete turnover from a low-diversity *Fabalitypris*-dominated pre-extinction community to a more diverse *Bairdiacypris*-dominated post-extinction community. The turnover coincides with the significant temperature increase that was previously recorded from north-west Iranian sections. The low diversity in the horizon immediately below the extinction horizon indicates that environmental changes, such as thermal stress, may have had an impact on the ostracod assemblages prior to the extinction event. In comparison with other diverse ostracod assemblages from the Palaeotethyan realm, the ostracods of the Aras Valley section are not associated with microbialites.

Key words: Ostracods, Iran, end-Permian, extinction, diversity, thermal stress.

THE environmental conditions during the end-Permian mass extinction event (EPME), and the environmental parameters that could have triggered the most severe biodiversity crisis in the Phanerozoic, are still a matter of debate. A valuable fossil group in the study of the nature of the extinction event is the Ostracoda, which has been studied in various sections around the world. Diversity patterns of ostracods in successions including the EPME are important for our understanding of the changing palaeoenvironmental conditions during this event, given that they may indicate fluctuations in salinity and oxygen content of the seawater. The most common scenarios for explaining the extinction include the combination of several effects (on temperature, oxygen content, seawater pH), all induced by the eruption of the Siberian Traps (Erwin 1994; Kidder & Worsley 2004; Svensen *et al.* 2009; Burgess & Bowring 2015; Bond & Grasby 2017). In the marine realm, the effects of the volcanism are

summarized as the ‘deadly trio’ (Bijma *et al.* 2013): (1) the recurring expansion of oceanic anoxic zones (Wignall & Twitchett 1996; Isozaki 1997; Brennecke *et al.* 2011; Song *et al.* 2012; Grasby *et al.* 2013; Clarkson *et al.* 2016; Lau *et al.* 2016; Zhang *et al.* 2018); (2) high-magnitude global warming (Joachimski *et al.* 2012; Sun *et al.* 2012; Schobben *et al.* 2014; Song *et al.* 2014); and (3) acidification of the ocean water (Payne *et al.* 2007; Hinojosa *et al.* 2012).

The study of Recent and fossil ostracods and their habitats has contributed significantly to ecological studies of historical and geological time scales. The taxonomic distribution of ostracods provides insights into the ecological state and the stability of an environment (Boomer *et al.* 2003; Yasuhara *et al.* 2003; Crasquin *et al.* 2010; Forel *et al.* 2013). Furthermore, occurrences of certain taxa can serve as a proxy for environmental parameters, such as trophic conditions or salinity (Forel *et al.* 2011;

Horne *et al.* 2011). For this reason, sedimentary successions covering the EPME in the Palaeotethys have already been studied intensively for their ostracod content (Wang 1978; Chen & Shi 1982; Shi & Chen 1987, 2002; Hao 1996; Crasquin-Soleau *et al.* 2004a, b, 2006a, b; Crasquin-Soleau & Kershaw 2005; Crasquin *et al.* 2008, 2010; Mette 2008, 2010; Liu *et al.* 2010; Forel & Crasquin 2011; Forel 2012, 2014; Forel *et al.* 2013, 2015; Wan *et al.* 2019). Griesbachian ostracods were found almost exclusively associated with microbialites (Forel *et al.* 2009, 2013, 2015; Forel 2012, 2014), which led to the hypothesis that a microbial refuge allowed the ostracods to survive the possibly adverse environmental conditions, such as anoxic or dysoxic phases (Forel *et al.* 2013). In the absence of microbialites, adverse conditions in the aftermath of the EPME generally led to low abundances and low diversity of ostracod assemblages (Crasquin & Forel 2014), and hence taxonomy and diversity patterns of this time interval are difficult to study at the species level. The preservation of the material is often poor and hampers identification at the species level. With the investigation of the Aras Valley section (north-west Iran), we are able to record ostracod occurrences before, during and after the extinction in a complete succession without sedimentary gaps (Ghaderi *et al.* 2014a; Leda *et al.* 2014; Gliwa *et al.* 2020a). The rock interval immediately above the extinction horizon is a shale succession with very high and relatively diverse ostracod content. Furthermore, the ostracod succession can be correlated with the evolutionary history of other fossil groups such as conodonts (Ghaderi 2014; Ghaderi *et al.* 2014a), ammonoids (Ghaderi *et al.* 2014a; Korn *et al.* 2016; Kiessling *et al.* 2018; Gliwa *et al.* 2020a) and brachiopods (Ghaderi *et al.* 2014b). In this study we describe, for the first time, the taxonomic characteristics of ostracods at the EPME interval in the Aras Valley section; this will allow the investigation of palaeoenvironmental changes that can be linked to the extinction event.

GEOLOGICAL SETTING

The Aras Valley section (39.015°N, 45.434°E), which was described in detail by Gliwa *et al.* (2020a), is located c. 19 km north-west of the towns of Julfa (or Jolfa, East Azerbaijan Province, Iran) and Dzhulfa (or Culfa, Nakhichevan province, Azerbaijan). The outcrop has a position 2 km to the north-west of the Dorasham 1 section of Ruzhencev *et al.* (1965) (Fig. 1).

During the Lopingian, north-west Iran was positioned at the north-western margin of the Sanandaj–Sirjan Terrane of the Cimmerian microcontinent, located between Neotethys and Palaeotethys. The investigated section was located at a latitude close to the equator (Fig. 1; e.g.

Stampfli & Borel 2002; Muttoni *et al.* 2009). At the EPME, the Sanandaj–Sirjan Terrane with the north-west Iranian sections was largely covered by a shallow to moderately deep sea. The north-west Iranian sediments are mostly composed of open sea deposits from an outer shelf setting (Kozur 2007; Leda *et al.* 2014; Gliwa *et al.* 2020a).

The sedimentary succession of the Aras Valley section, which belongs to a north-inclined monocline, is mainly composed of Wuchiapingian–Griesbachian sedimentary rocks, exposed across a lateral extension of 200 m. The exposed succession has a total thickness of 37 m including the extinction horizon and the Permian–Triassic boundary (PTB; Fig. 2). A comprehensive biostratigraphic investigation of the section, including detailed documentation of ammonoid and conodont occurrences, was carried out by Ghaderi *et al.* 2014a and Gliwa *et al.* 2020a. The position of the extinction horizon (set as 0.00 m) is, as in other Iranian PTB sections, defined at the top of the *Paratirolites* Limestone at the transition to the argillaceous Aras Member ('Boundary Clay'), which corresponds to the transition from the *Clarkina hauschkei* zone to the *Hindeodus praeparvus*–*H. changxingensis* zone (Fig 2; Kozur 2005, 2007; Ghaderi *et al.* 2014a; Leda *et al.* 2014; Gliwa *et al.* 2020a). Detailed facies investigation of the Aras Valley section (Gliwa *et al.* 2020a) and of the neighbouring Ali Bashi section (Leda *et al.* 2014), furthermore, indicates a sudden decrease of skeletal carbonate producers as well as the complete disappearance of cephalopods and other macrofossils above the *Paratirolites* Limestone, which confirms the position of the extinction horizon. In contrast to the other north-west Iranian sections, the shale-dominated post-extinction horizon (Aras Member) has a relatively larger thickness of 2.50 m, which enables detailed investigation of the extinction interval. The PTB, marked by the first occurrence of the conodont species *Hindeodus parvus*, is located at the base of the *Claraia* Beds at +2.55 m (Fig. 2; Ghaderi *et al.* 2014a).

Several north-west Iranian PTB sections (Ali Bashi, Zal) have been investigated in detail for their conodont biostratigraphy (Kozur 2005, 2007; Shen & Mei 2010; Ghaderi *et al.* 2014a). These studies demonstrated that the succession of conodont zones does not lack any of the zones recognized in other regions such as South China. As shown by Gliwa *et al.* (2020a), the Aras Valley section very closely resembles the Ali Bashi and Zal sections, both in lithology and stratigraphic succession of conodont zones, reflecting the completeness of the stratigraphic succession. Furthermore, the $\delta^{13}\text{C}_{\text{carb}}$ curve of the Aras Valley section parallels that of other sections and does not show any evidence for a stratigraphic gap (Gliwa *et al.* 2020a).

In the present study, we focus on the interval from –3.80 m to +7.00 m with respect to the extinction



FIG. 1. Palaeogeographical position of north-west Iran during the late Permian (modified from Stampfli & Borel 2002) and geographical position of Permian–Triassic boundary sections in the Transcaucasus and in north-west Iran (from Arakelyan *et al.* 1965). Relevant sections are numbered as follows: 1, Aras Valley; 2, Dorasham 1; 3, Dorasham 2; 4, Kuh-e-Ali Bashi; 5, Zal. Colour online.

horizon. This includes the pre-extinction interval of the Ali Bashi Formation (Changhsingian) and the post-extinction interval of the Elikah Formation (latest Changhsingian – Griesbachian). The lithostratigraphic scheme for the Transcaucasus region was developed by Stepanov *et al.* (1969) and Ghaderi *et al.* (2014b) and is described in detail for the Aras Valley section in Gliwa *et al.* (2020a). The interval studied here for ostracods has a thickness of 10.80 m and includes the following three lithological units.

1. *Paratirolites* Limestone (late Changhsingian): together with the underlying Zal Member, this forms the Ali Bashi Formation. It is composed of red to purple nodular limestone and has a total thickness of 4.60 m. Its upper limit is marked by the abrupt change from carbonates to shales at the base of the overlying Aras Member. The top 4 cm of the member

is marked by conspicuous bioturbation; a dense accumulation of keratose sponge remains occurs in the upper 2 cm (Gliwa *et al.* 2020a). The extinction event was interpreted to have taken place between the first occurrence of the keratose sponges and the initial deposition of the ‘Boundary Clay’ (Aras Member; Gliwa *et al.* 2020a).

2. Aras Member (‘Boundary Clay’; latest Changhsingian): it is the lowest member of the Elikah Formation and consists of 2.50 m-thick purple and light grey shales with a few marly intercalations. The deposition of this shale horizon is interpreted as the result of a drastic decrease of carbonate production (Richoiz *et al.* 2010; Leda *et al.* 2014).
3. *Claraia* Beds (earliest Griesbachian): only the basal 4.50 m of the *Claraia* Beds was logged in the present study; the entire member reaches a total thickness of

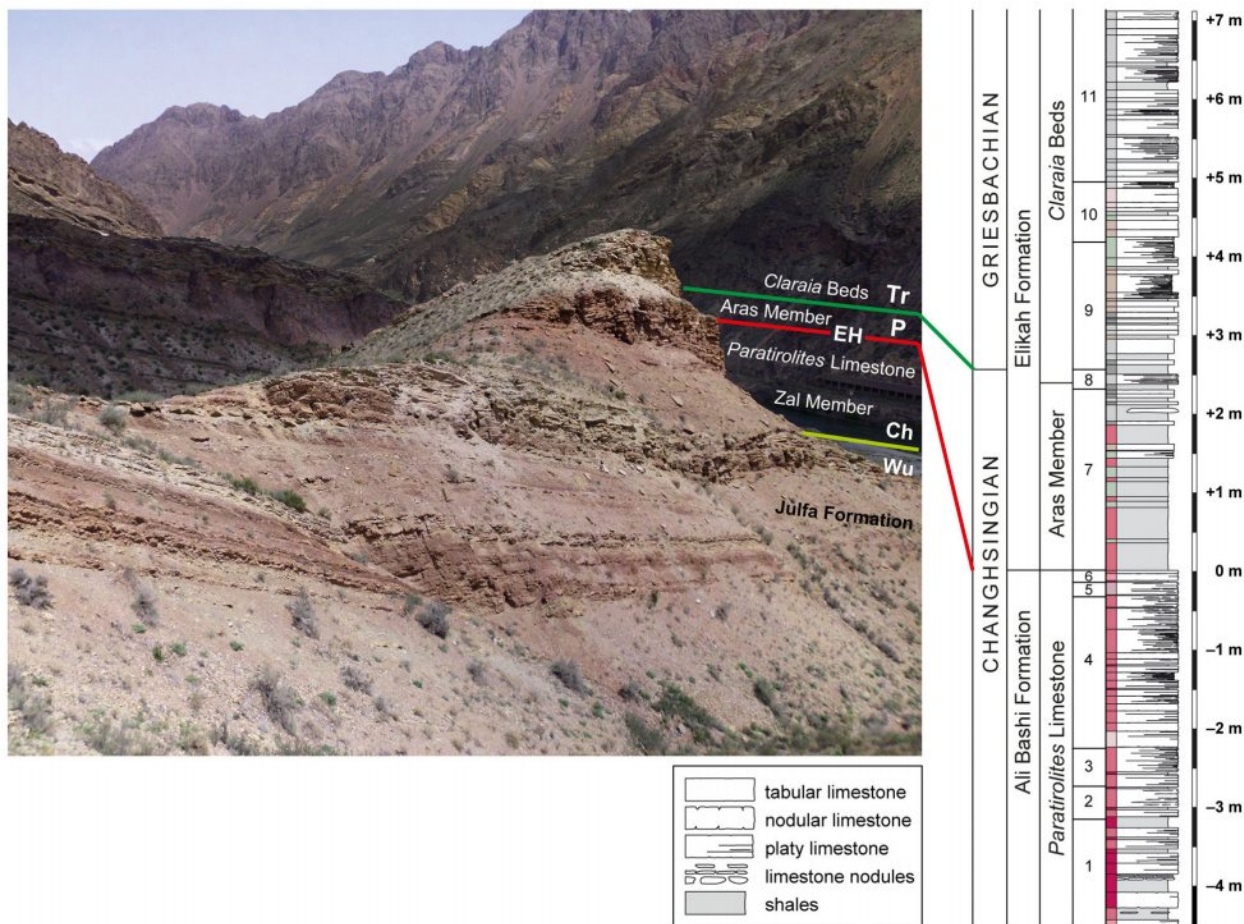


FIG. 2. Aras Valley section (north-west Iran) with lithological column for the sampled interval. Conodont zones are numbered as follows: 1, *Clarkina changxingensis*; 2, *Clarkina bachmanni*; 3, *Clarkina nodosa*; 4, *Clarkina yini*; 5, *Clarkina abadehensis*; 6, *Clarkina hauschkei*; 7, *Hindeodus praeparvus*–*Hindeodus changxingensis*; 8, *Merrillina ultima*–*Stepanovites ?mostleri*; 9, *Hindeodus parvus*; 10, *Isarcicella staeschei*; 11, *Isarcicella isarcica*. View towards the north. In the background, mountains in Azerbaijan consisting of Triassic rocks. *Abbreviations:* Ch, Changhsingian; EH, extinction horizon; P, Permian; Tr, Triassic; Wu, Wuchiapingian. Colour online.

approximately 280 m in the Ali Bashi Mountains (Stepanov *et al.* 1969). The *Claraia* Beds are composed of mostly grey to beige platy limestone beds with shale intercalations.

OSTRACOD STUDIES IN THE TRANSCAUCASIAN REGION

In the present study, we investigated the ostracod succession of the Aras Valley section. The studied interval covers almost the entire Lopingian *Paratirolites* Limestone, the extinction horizon, the Aras Member and the lower part of the Induan *Claraia* Beds (Fig. 2). The Dorasham 2 section, which is very similar in the lithological succession (e.g. Zakharov 1992), is located c. 10 km towards the East on the northern side of the Araxes River in the

Nakhichevan province of Azerbaijan (Fig. 1). This section was investigated for its ostracod content by Belousova (1965); she studied 500 specimens that were assigned to 26 species. The stratigraphic resolution in that study was, however, very coarse; Belousova (1965) separated only two units ('Dzhulfian' and 'Induan'), of which the latter includes most of the Zal Member plus the *Paratirolites* Limestone. The ostracod assemblages of both units show the same diversity. Most of the identified species in that study belong to smooth forms of the family Bairdiidae.

A more detailed stratigraphic assignment was provided by Kotlyar *et al.* (1983). They separated the 'Induan' unit by Belousova (1965) into five subunits, of which the lower four belong in the Zal Member. The topmost of the five is the *Paratirolites* Limestone, which was regarded as one single unit. According to Kotlyar *et al.* (1983), the diversity decreases from c. 20 species to only four species

during the ‘Dorashamian’ (= Changhsingian) interval. Both Belousova (1965) and Kotlyar *et al.* (1983) described only the succession below the extinction horizon (as shown by Zakharov 1992), precluding any statement on the influence of the extinction event itself.

The Zal section, which is located *c.* 35 km south-east of the Aras Valley section and 24 km south of Julfa (Fig. 1), was studied by Mette (2008, 2010) with a focus on the ostracod assemblages on both sides of the extinction horizon. He described a complete faunal turnover at the extinction horizon and a post-extinction assemblage of the ‘Boundary Clay’, which is of low diversity and dominated by a single species of the genus *Indivisia*.

MATERIAL AND METHOD

For ostracod abundance data and taxonomy, we prepared a total of 59 samples, ranging from 0.4 to 1 kg. Samples from limestone and marly limestone beds (*c.* 0.4 kg each) were processed using hot acetolysis following Crasquin-Soleau & Kershaw (2005). For the wet sieving process, we used two sieves with 1.5 mm and 0.063 mm mesh sizes to remove the coarse fractions from the residue. Very soft shale samples (1 kg each) from the Aras Member were processed only with water before the wet sieving process. Ostracod specimens of 45 of the 59 sample horizons were identified. The remaining 14 sample horizons yielded ostracods but were not analysed to the species level. In order to obtain a representative sample of the ostracod assemblages, only samples with more than 40 identified specimens were used for calculating the species richness. An investigation of internal taxonomic features was not possible because of the preservation of the specimens with sparry calcite infill; hence we assumed that the largest specimens of a species represent the adult stage.

Most of the ostracods recovered from the studied samples have smooth external surfaces lacking informative elements such as ornamentation. As a consequence, our taxonomic investigation relies on traditional morphological measurements of the length and height of the carapaces and valves. Other morphological characters such as the position of maximum length and height have also been determined and compared for species delimitation. All taxonomic analysis and discussions performed have been quantified as much as possible with, for example, measurements of angles and relative length proportions of individual features such as dorsal or ventral border.

For the validation of the species identification and for illustration of different ontogenetic stages within a species, all specimens assigned to a new species and some selected examples of already described species were plotted in a length/height (L/H) diagram. The ontogenetic stages below the adult stage are abbreviated to ‘A’ with a running

number in the direction of the smallest instars. The stratigraphic position of individual specimens and the range of species are given in metres from the base of the extinction horizon (top surface of the *Paratirolites* Limestone).

SYSTEMATIC PALAEOLOGY

Only the ten newly introduced species are fully described in detail here. Remarks are given for some taxa, defined from other sections; all other species are figured. We use the systematic classification proposed by Moore (1961) and modified by Horne *et al.* (2002). All specimens are permanently stored in the micropalaeontology collection of the Museum für Naturkunde, Berlin, Germany. The material is stored in cardboard slides or glued on scanning electron microscopy pads. All type specimens are stored in cardboard slides and have a unique catalogue number with the prefix ECO. All other displayed specimens are stored under a sample identifier consisting of the sample name and a successive number (AV prefix referring to the Aras Valley section), followed by the sample depth in centimetres (‘n’ for negative values) and the preparation batch (if present).

Abbreviations. AB, anterior border; ADB, anterodorsal border; AVB, anteroventral border; DB, dorsal border; H, height; H_{max}, maximum height; L, length; L_{max}, maximum length; LV, left valve; PB, posterior border; PDB, posterodorsal border; PVB, posteroventral border; RV, right valve; VB, ventral border; W, width; W_{max}, maximum width. The dimensions used in the species description refer to the specimen with the smallest and largest dimensions in each species.

Class OSTRACODA Latreille, 1806
 Subclass PODOCOPA Müller, 1894
 Order PODOCOPIDA Sars, 1866
 Suborder BAIRDIOCOPINA Gründel, 1967
 Superfamily BAIRDIOLIDEA Sars, 1887
 Family BAIRDIIDAE Sars, 1887
 Genus FABALICYPRIS Cooper, 1946

Type species. *Fabalitypris wileyensis* Cooper, 1946, by original designation.

Fabalitypris obunca Belousova, 1965
 Figure 3A–C

- 1965 *Fabalitypris obuncus* Belousova, p. 264, pl. 50, fig. 5a, b.
 1965 *Fabalitypris hoxabarensis* (Harlton); Belousova, pl. 50, fig. 6a, b.

Material. 732 complete carapaces (L = 221–883 µm).

Remarks. The late Permian specimens identified as ‘*Fabalitypris hoxbarensis* Harlton’ by Belousova (1965) from the neighbouring Dorasham section (Azerbaijan) were erroneously attributed to that species. The drawing of the holotype of *Fabalitypris hoxbarensis* by Harlton (1927) shows a very pronounced pointed posterior end and large overlap at DB and VB, which is not the case in the illustrated specimen in Belousova (1965). Furthermore, the DB by Harlton (1927) is nearly straight in comparison to the uniformly convex DB displayed in Belousova (1965). Given that the carapace outline in lateral and dorsal view is very similar, we assign these specimens to *F. obunca*, which is described to have a strong intraspecific variability (Belousova 1965).

Fabalitypris obunca is very similar in its overall appearance to *Fabalitypris parva* Wang, 1978, which was found in various late Permian successions from the Palaeotethys (Wang 1978; Shi & Chen 1987; Crasquin-Soleau *et al.* 1999, 2004b; Mette 2008; Crasquin *et al.* 2010; Forel 2012; Forel *et al.* 2013, 2015). A synonymy of *F. parva* and *F. obunca* may be considered, but this is a topic beyond this study.

Occurrence. Dorasham, Azerbaijan, Wuchiapingian–Changhsingian (Belousova 1965); Aras Valley, *Paratirolites* Limestone (Changhsingian), from –3.80 to –0.01 m (Fig. 4).

Fabalitypris cf. minuta Cooper, 1946

Figures 3H–L, 5

cf. 1946 *Fabalitypris minuta* Cooper, p. 60, pl. 5, figs 31–32.

Material. 85 complete carapaces (L = 452–1214 µm).

Remarks. The L/H diagram of the specimens from our material enables a distinction of five ontogenetic stages (A-4 juvenile stage to adult stage, Fig. 5). The Aras Valley material is, with respect to the lateral and dorsal outlines of the carapaces, similar to the Pennsylvanian *Fabalitypris minuta* Cooper, 1946 from Illinois (Cooper 1946). The specimen described by Cooper (1946) is c. 200 µm shorter than our material of the adult stage; it would fit in the range of the A-1 instars of our material (Fig. 5). Our material shows strong intraspecific variation, noticeable in the carapace H/L ratio and the posterior and ventral overlapping

areas. The preservation of our material does not allow an unequivocal attribution to *F. minuta*, given that the overlapping area in our specimens appears indistinct. Changhsingian specimens attributed to *F. minuta* were recorded at Meishan, South China (Shi & Chen 1987; Crasquin *et al.* 2010).

Occurrence. Aras Valley; Aras Member (Changhsingian), from +0.05 to +0.60 m (Fig. 4).

Fabalitypris veronicae Gliwa sp. nov.

Figures 3M–Q, 6

LSID. urn:lsid:zoobank.org:act:B0C4661D-6AB1-43E2-BBD0-F7063C6EEFB7

Derivation of name. Named after Veronica Piazza, honouring her encouragement during the progress of this work.

Type specimens. Holotype: complete carapace ECO104 (Fig. 3M, N), sample AV028. Paratype: complete carapace ECO105 (Fig. 3O, P), sample AV015.

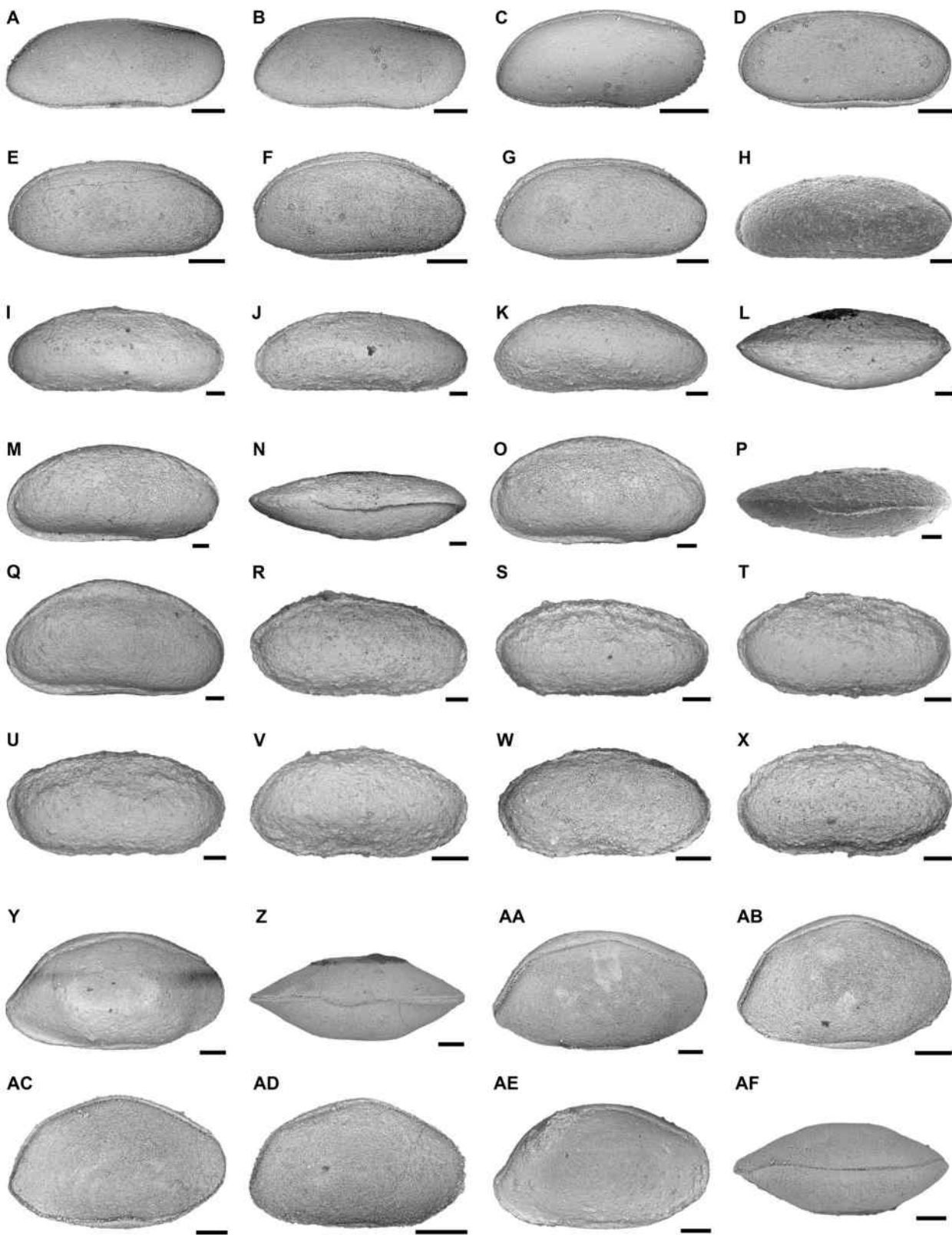
Type locality and horizon. Aras Valley; Aras Member (Changhsingian), +0.28 m.

Material. 69 complete carapaces (L = 461–1285 µm; Fig. 6).

Diagnosis. Species of *Fabalitypris* with straight and horizontal DB at RV, elongate symmetrical carapace in lateral view and slender in dorsal view.

Description. Carapace elongate, subreniform in lateral view with H_{max} located at mid-L; slender (W/L c. 0.30–0.33) in dorsal view with acuminate anterior end and largest width in the posterior third. Overlap of larger left valve all around the right valve; overlap thinner along AVB and more pronounced at ventral and posterior margin. Dorsal margin uniformly convexly rounded at LV; DB straight, horizontal and long (c. 50% of L_{max}) at RV. Distinct angulations between DB and ADB as well as between DB and PDB (both c. 150°). ADB straight to slightly concave;

FIG. 3. SEM micrographs of ostracods from the Aras Valley section, north-west Iran. A–C, *Fabalitypris obunca* Belousova, 1965: A, AVn023-66, right lateral view; B, AVn023-27, right lateral view; C, AVn023-75, right lateral view. D–G, *Fabalitypris blumenstengeli* Crasquin *in* Crasquin *et al.*, 2008: D, AVn008-16, right lateral view; E, AVn008-07, right lateral view; F, AVn062-63, right lateral view; G, AVn040-160, right lateral view. H–L, *Fabalitypris cf. minuta* Cooper, 1946: H, AV028YTE-17, right lateral view; I, AV028YSH-35, right lateral view; J, AV028YTE-01, right lateral view; K, AV028YSH-36, right lateral view; L, AV028YTE-01, ventral view. M–Q, *Fabalitypris veronicae* Gliwa, sp. nov.: M–N, holotype ECO104; M, right lateral view; N, ventral view; O–P, AV028YTE-18; O, right lateral view; P, ventral view; Q, paratype ECO105, right lateral view. R–S, *Fabalitypris* sp. 1: R, AV116SH-56, right lateral view; S, AV265SH-80, right lateral view. T–U, *Fabalitypris* sp. 2: T, AV288SH-145, right lateral view; U, AV288SH-144, right lateral view. V–X, *Fabalitypris* sp. 3: V, AV116Y-32, right lateral view; W, AV288SH-92, right lateral view; X, AV116SH-13, right lateral view. Y–AF, *Orthobairdia capuliformis* Gliwa, sp. nov.: Y–Z, holotype ECO106: Y, right lateral view; Z, ventral view; AA paratype ECO107, right lateral view; AB, AVn62-09, right lateral view; AC, AVn62-31, right lateral view; AD, AVn62-20, right lateral view; AE, AVn25-26, right lateral view; AF, AVn62-56, dorsal view. Scale bars represent 100 µm.



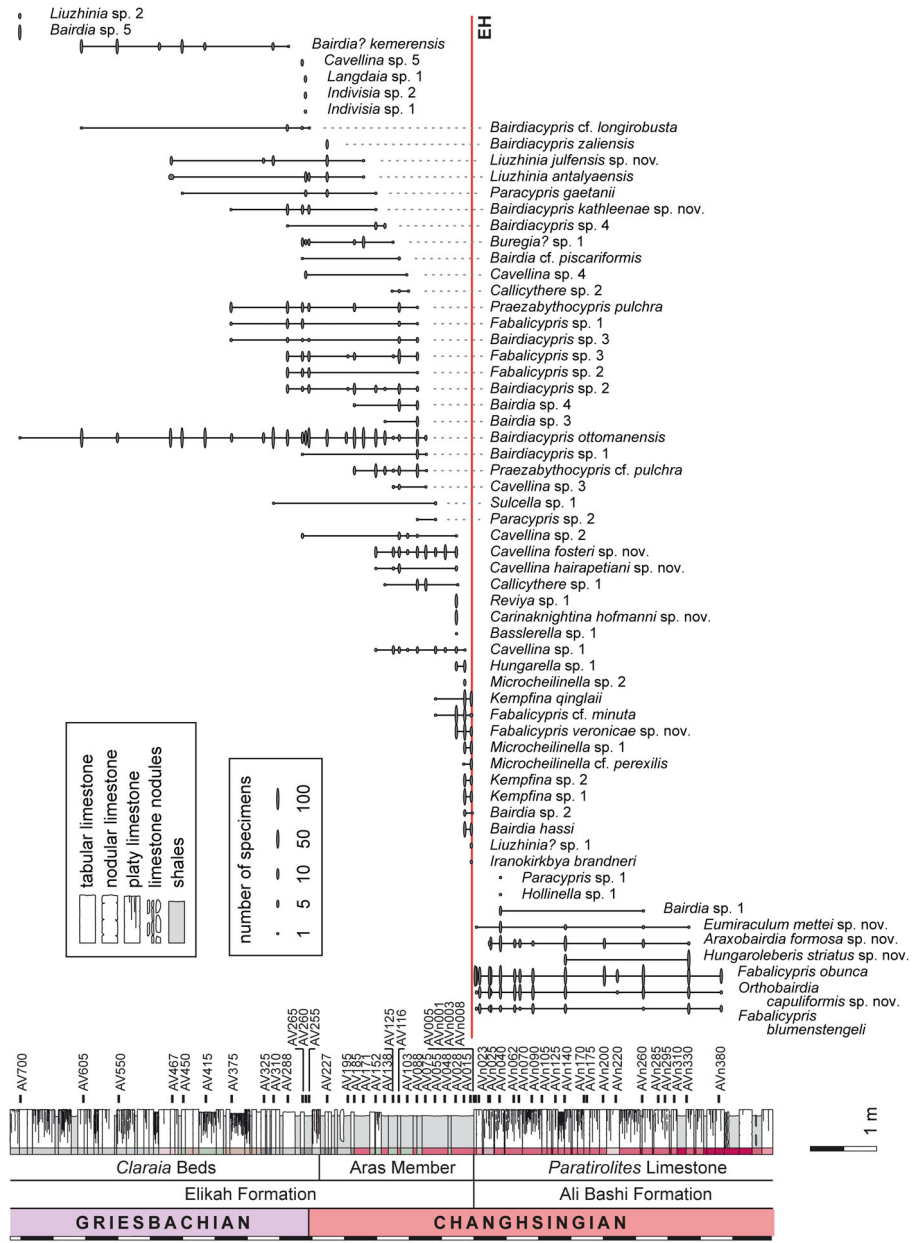
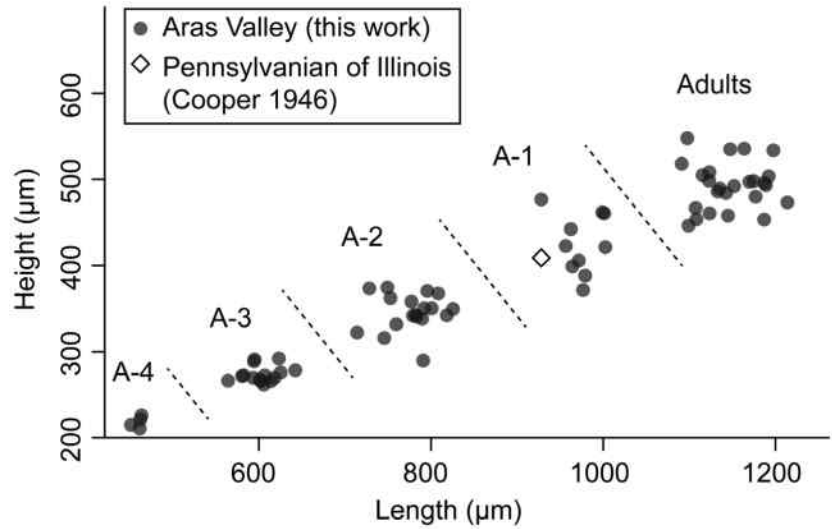


FIG. 4. Distribution of analysed samples in the lithological column of the Aras Valley section. Occurrences of ostracod specimens per species are displayed by their symbol width. Abbreviation: EH, extinction horizon. Colour online.

FIG. 5. Length/height scatter plot comparing *Fabalitypris* cf. *minuta* Cooper, 1946 from the Aras Valley with the specimen of *Fabalitypris minuta* described in Cooper (1946).



anterior and posterior maximum of convexity at lower third of H_{max} . Posterior end slightly more broadly rounded than anterior end. Surface smooth.

Remarks. The species is very similar to the early Permian *Bairdiacypris ventralis* Chen, 1958 from South China, particularly in the general outline of the carapace and the angulations of the dorsal margin. The specimens of Chen & Shi (1982) would plot, in the L/H diagram, in the range of the stages A-2, A-1 and adults of *F. veronicae* (Fig. 6). However, the present specimens are slenderer in dorsal view ($W/L = 0.30-0.33$, compared with $W/L c. 0.40$ in the illustrated specimens of Chen 1958). The ventral view of the new species indicates a clear offset of the ventral overlap in the anterior half of the carapace, which

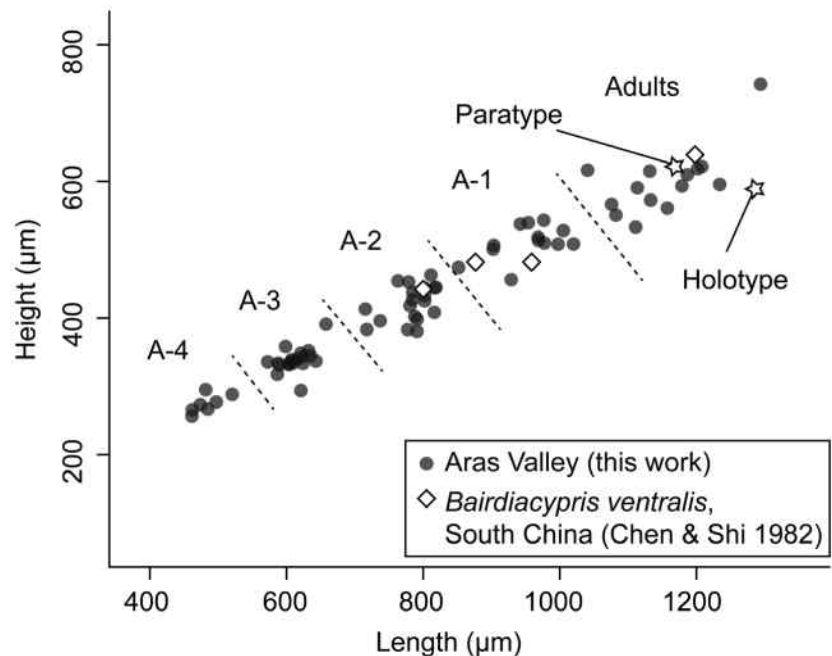
is typical for *Fabalitypris* (Fig. 3N, P). A ventral view was not illustrated for *Bairdiacypris ventralis* in Chen & Shi (1982); such a ventral structure is also neither mentioned in the original description nor clearly visible in the original illustrations of this species in Chen (1958).

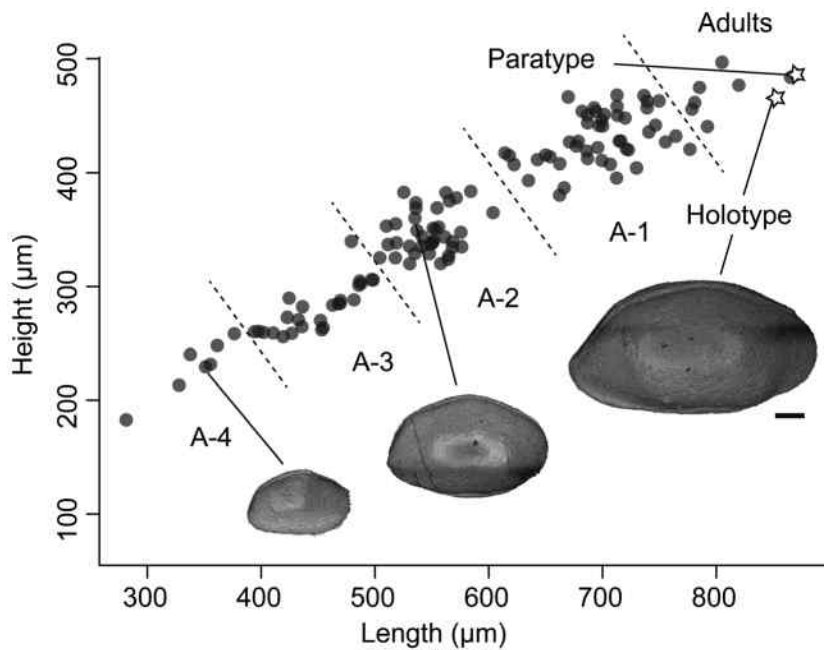
Occurrence. Aras Valley; Aras Member (Changhsingian), from +0.05 to +0.28 m (Fig. 4).

Genus ORTHOBAIRDIA Sohn, 1960

Type species. *Bairdia cestriensis* Ulrich, 1891; subsequently designated by Sohn (1960).

FIG. 6. Length/height scatter plot comparing *Fabalitypris veronicae* Gliwa, sp. nov. from the Aras Valley section with specimens of *Bairdiacypris ventralis* Chen, 1958 from Chen & Shi (1982).





Orthobairdia capuliformis Gliwa sp. nov.
Figures 3Y–AF, 7

LSID. urn:lsid:zoobank.org:act:911A476B-9A4C-4E59-8C83-C51EF1885374

Derivation of name. From Latin *capulus* = coffin; after outline shape of the carapace in dorsal view.

Type specimens. Holotype: complete carapace ECO106 (Fig. 3Y, Z), sample AVn023. Paratype: complete carapace ECO107 (Fig. 3AA), sample AVn062.

Type locality and horizon. Aras Valley; *Paratirolites* Limestone (Changhsingian), at -0.23 m.

Material. 188 complete carapaces ($L = 281\text{--}870$ μm ; Fig. 7).

Diagnosis. A species of *Orthobairdia* with distinct dorsal angulations and large H/L ratio; slight concavity at the base of AVB; posterior end slightly tapered in lateral and dorsal view.

Description. Medium-sized specimens with sub-ovate outline in lateral view; fusiform with acuminate ends and almost parallel sides in dorsal view; H_{max} at the angulation between DB and ADB and L_{max} in the lower third of H; W_{max} distributed around the middle third of the carapace; W/L c. 0.40 in adult carapaces. Left valve overlaps right valve all around the carapace except for the anterior and posterior ends, widest overlap along DB and at oral concavity. Dorsal margin of right valve distinctively separated in three parts by uniform angulations; angulations in dorsal margin of left valve appear more rounded. Straight to slightly concave

FIG. 7. Length/height scatter plot of *Orthobairdia capuliformis* Gliwa, sp. nov. from the Aras Valley section. Displayed specimens from left to right: AVn062-27, AVn062-15, ECO106. Scale bar represents 100 μm .

DB bent towards the straight ADB with an angle of $135\text{--}140^\circ$. AB uniformly rounded with large radius of curvature, maximum around mid-H. Anterior end slightly tapered. Slight concavity in AVB; not present in A-4 instars (Fig. 7). Ventral margin of left valve uniformly convex with median oral concavity in the right valve. PVB slightly tapered with narrow lateral compression. PB narrowly rounded with maximum of convexity in the lower fourth of H. Posterior end bairdiid, slightly elongate, with concave PDB in adult specimens. Posterior end shorter, narrower with straight and steep PDB in juvenile specimens. PDB bent towards DB in an angle of $130\text{--}135^\circ$. Surface smooth.

Remarks. The juvenile specimens of *Orthobairdia capuliformis* have a stronger angulation in the right valve between DB and PDB than adult ones (Fig. 7). In juveniles (A-4 to A-1) the DB is bent towards the ADB at an angle of $123\text{--}135^\circ$ while it ranges from 140 to 145° in adult specimens. Compared with adult specimens, some juvenile specimens have a very thin overlap of the LV also at the posterior end (Fig. 3AC). The H/L ratio decreases throughout ontogeny: the mean H/L ratio in stage A-4 juveniles is 0.67 and decreases in A-3 to A-1 instars, which show very similar mean H/L ratios between 0.62 and 0.63; the mean H/L in adults decreases further to 0.58. The juvenile specimens are very similar to the late Permian *Silenites sasakwaformis* Shi in Shi & Chen, 1987, which is known from South China and the Central Alborz Mountains in Iran (Shi & Chen 1987; Crasquin *et al.* 2010; Forel *et al.* 2015). However, the AB in *S. sasakwaformis* is more broadly rounded and the posterior end is less bairdiid, as it is in the adult specimens of the new species. The adult specimens resemble the Lopingian *Orthobairdia zaliensis* Mette, 2010 from north-west Iran and Azerbaijan by their similar outline in dorsal view. However, the dorsal margin of *O. zaliensis* is not distinctively angulated and its H/L ratio is lower than that of *O. capuliformis*. The new species resembles, in its

lateral outline, the late Permian *Bairdia intermedia* Belousova, 1965 from the Dorasham section (Azerbaijan). However, *B. intermedia* is clearly diamond-shaped in dorsal view, in contrast to the typical *Orthobairdia* shape with its parallel middle part. Furthermore, *B. intermedia* has a uniformly rounded DB, whereas the angulations from DB to ADB and PDB are clearly visible. The specimens figured as *Bairdia rhomboidalis* Hamilton and *Bairdia anbeedei* Belousova by Belousova (1965) are both nearly identical to *O. capuliformis* in lateral view. The dorsal views for both species in Belousova (1965), however, show a fusiform to diamond-shaped carapace outline without a parallel middle part.

Occurrence. Aras Valley; *Paratirolites* Limestone (Changhsingian), from -3.80 to -0.03 m (Fig. 4).

Genus ARAXOBAIRDIA Gliwa nov.

LSID. urn:lsid:zoobank.org:act:DD77A055-09DB-487B-AA70-93A505731F73

Type species. *Araxobairdia formosa* sp. nov.

Derivation of name. Referring to the type locality at the Araxes (Aras) River.

Diagnosis. Genus of the family Bairdiidae with subfusiform carapace in lateral view. Hexagonal outline with subparallel sides and generally large width in dorsal view. Straight DB with shoulder-like depression at the PDB in lateral view. Fine horizontal striation on the carapace surface.

Assigned species. *Araxobairdia formosa* sp. nov.

Remarks. The new genus is attributed to the superfamily Bairdioidea because of the carapace features. Any other features that are indicative for this superfamily cannot be analysed in this material; the inner lamella with vestibulum is not visible, because the carapace is filled with sparry calcite or sediment and isolated valves are not well preserved; muscle scars and hinge are not preserved. The new genus shows typical carapace features of the family Bairdiidae: in lateral view, the carapace outline is rounded trapezoidal and has a uniformly angulated dorsal margin with slightly concave ADB and PDB leading to bairdiid anterior and posterior borders. Only *A. formosa* (this study) from the Changhsingian is hitherto attributed to this genus.

Araxobairdia formosa Gliwa sp. nov.

Figures 8A–H, 9

LSID. urn:lsid:zoobank.org:act:78EA6E7D-9CE7-48F4-8929-EAC6FE6D987C

Derivation of name. From the Latin *formosa* (beautiful).

Type specimens. Holotype: complete carapace ECO108 (Fig. 8A, G), sample AVn062. Paratype: complete carapace, ECO109 (Fig. 8E), sample AVn062.

Type locality and horizon. Aras Valley; *Paratirolites* Limestone (Changhsingian), -0.62 m.

Material. 68 complete carapaces ($L = 374\text{--}742$ μm ; Fig. 9), 25 single valves and 14 fragments.

Diagnosis. Species of *Araxobairdia* with striated carapace surface, longitudinal shallow ribs merging into the posterior and anterior ends. Carapace subfusiform in lateral view with uniformly angulated dorsal margin and hexagonal outline with subparallel sides in dorsal view.

Description. Subfusiform carapace with symmetric trapezoidal outline in lateral view; H_{max} and W_{max} distributed along the middle third of L_{max} . Hexagonal outline with subparallel sides and generally large width ($W/L = 0.56\text{--}0.58$) in dorsal view. Plump carapace shape with laterally inflated valves and large flat ventral surface. Shallow shoulder-like depression at the antero- and posterodorsal lateral surface, more distinct at the PDB. L_{max} in the lower half of the H_{max} . Left valve overlaps right valve all around the carapace, with dorsal offset at the angulations between PDB and DB as well as between DB and ADB (visible in dorsal view; Fig. 8G). The tripartite dorsal margin is distinct at both valves. DB long (one-third of L_{max}), slightly convex in right valve and straight to slightly concave in left valve. DB gently bent towards ADB (c. 150°). Straight PDB bent against the DB at c. 145° . AB uniformly rounded with maximum of convexity below mid-H. Ventral margin uniformly convex in left valve and slightly concave in the median portion of right valve. PB has a narrower radius of curvature than AB, with maximum of convexity located at the lower third of H_{max} . Carapace surface striated on the lateral and dorsal surface with 13–14 longitudinal ribs that merge in the posterior and anterior ends. Ventral ribs run uniformly convex and parallel to the ventral margin, dorsal ribs are tripartite and run parallel to the dorsal margin. The ribs in the median area are almost straight. Striation on the ventral side less pronounced with almost smooth surface in the central ventral area.

Remarks. It is not possible to define boundaries between different ontogenetic stages in the L/H diagram; most of the specimens plot in a continuous scatter line (Fig. 9). However, there are clear morphological differences between adults and juveniles: juveniles generally show a more uniformly rounded dorsal margin, a larger radius of curvature at the AB and H_{max} located slightly behind mid-L (Fig. 9).

Strongly ornamented representatives of the Bairdiidae, such as *Abrobairdia*, *Ceratobairdia*, *Petasobairdia*, *Ptychobairdia* from the Permian–Triassic transitional time interval display typical Mesozoic–Cenozoic affinities (Crasquin & Forel 2014). Elongated ornamentation, such as lateral horizontal ridges are for example present in *Abrobairdia* Chen *in* Chen & Shi, 1982 (e.g. the Changhsingian *A. brevicosta* Chen & Shi, 1982 from South China) and in *Ptychobairdia* Kollmann, 1960 (e.g. *P. ruttneri*

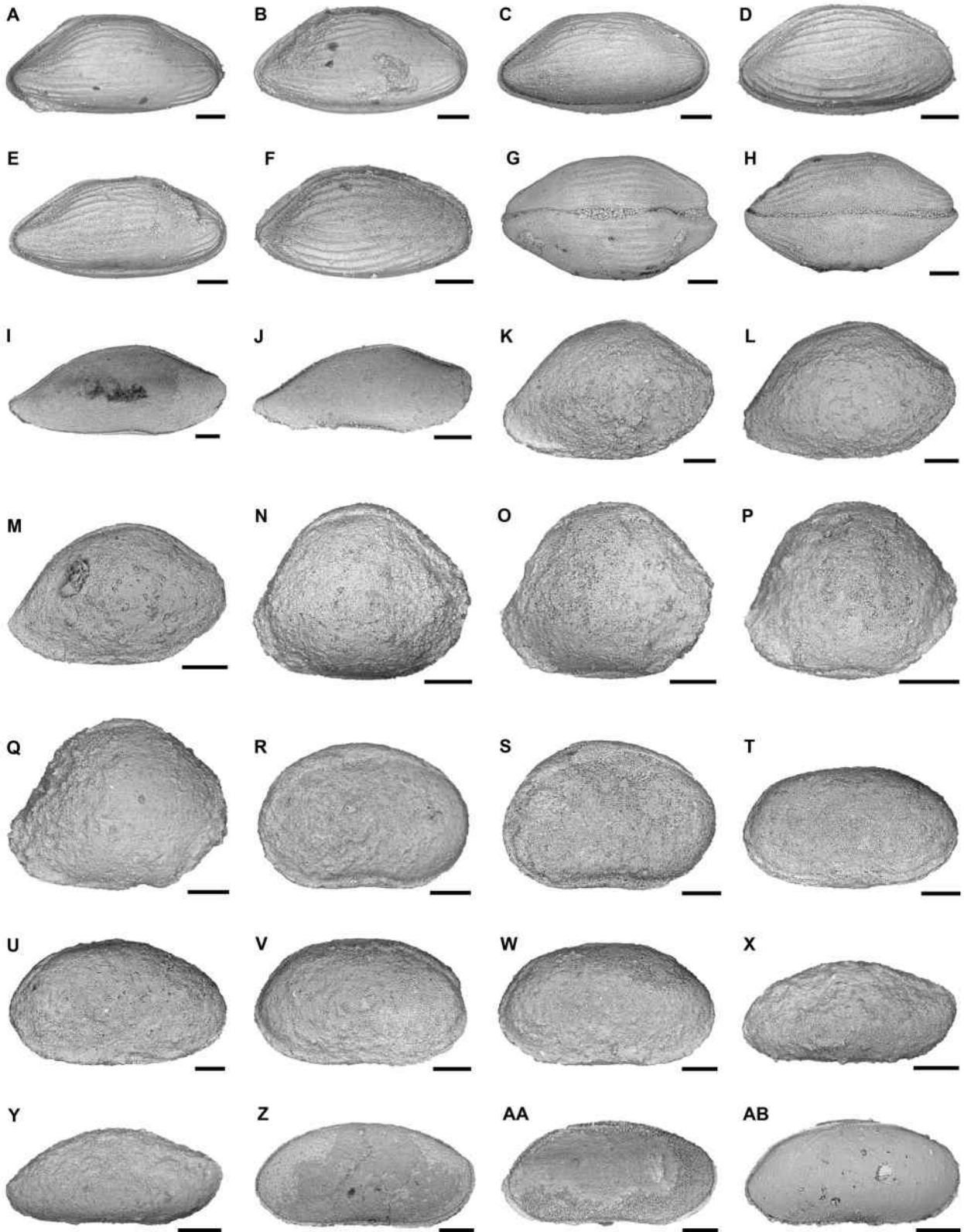


FIG. 8. SEM micrographs of ostracods from the Aras Valley section, north-west Iran. A–H, *Araxobairdia formosa* Gliwa, sp. nov.: A, holotype ECO108, right lateral view; B, AVn025-17, right lateral view; C, AVn070-30, right lateral view; D, AVn040-92, right lateral view; E, paratype ECO109, right lateral view; F, AVn040-111, right lateral view; G, holotype ECO108, dorsal view; H, AVn062-02, ventral view. I–J, *Bairdia* sp. 1: I, AVn040-176, right lateral view; J, AVn040-26, right lateral view. K–M, *Bairdia hassi* Sohn, 1960: K, AV015YTE-22, right lateral view; L, AV005XTE-32, right lateral view; M, AV015YTE-10, right lateral view. N–Q, *Bairdia* sp. 2: N, AV015TE-88, right lateral view; O, AV015Z-67, right lateral view; P, AV015Z-68, right lateral view; Q, AV005X-13, right lateral view. R–S, *Bairdia* sp. 3: R, AV088-90, right lateral view; S, AV088-201, right lateral view. T–W, *Bairdia* sp. 4: T, AV185TE-137, right lateral view; U, AV116SH-12, right lateral view; V, AV116SH-91, right lateral view; W, AV116SH-25, right lateral view. X–Y, *Bairdia* cf. *piscariformis* Chen, 1958: X, AV265XSH-06, right lateral view; Y, AV116Y-37, right lateral view. Z–AB, *Bairdia? kemerensis* Crasquin-Soleau, 2004: Z, AV310-36, right lateral view; AA, AV310-54, right lateral view; AB, AV467-21, right lateral view. Scale bars represent 100 μ m.

Kristan-Tollmann, 1991 from north-east Iran). However, with the fine horizontal striation of the carapace surface and its large width, together with the shoulder-like depression at the PDB, *A. formosa* has a unique appearance among the Bairdiidae.

Occurrence. Aras Valley; *Paratirolites* Limestone (Changhsin-gian), from -3.30 to -0.23 m (Fig. 4).

Genus BAIRDIA McCoy, 1844

Type species. *Bairdia curta* McCoy, 1844; subsequently designated by Ulrich & Bassler (1923).

Bairdia? kemerensis Crasquin-Soleau in Crasquin-Soleau et al., 2004b
Figures 8Z–AB, 10A–C, 11

2004b *Bairdia? kemerensis* Crasquin-Soleau in Crasquin-Soleau et al., p. 285, pl. 2, figs 1–5.

2014 *Bairdia? kemerensis* Crasquin-Soleau; Forel, p. 7, text-fig. 4B–I.

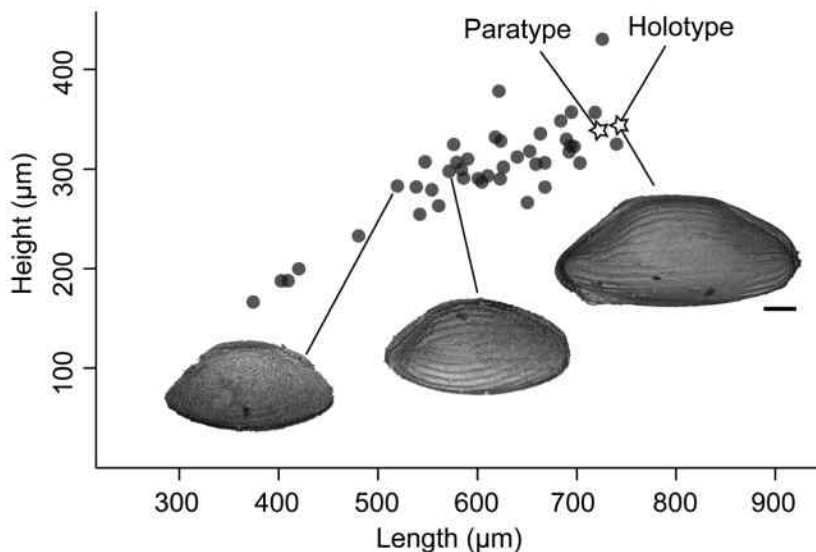
2019 *Bairdia? kemerensis* Crasquin-Soleau; Wan et al., p. 6, text-fig. 3.13.

Material. 76 complete carapaces ($L = 301$ – 654 μ m; Fig. 11).

Remarks. The ontogenetic stages of *B.? kemerensis* differ mainly in the position and shape of the PB, which was already investigated by Forel (2014): with progressing ontogeny, the posterior maximum of convexity migrates dorsally and the PB generally becomes wider (Fig. 11). The studied specimens show, furthermore, a decrease in the H/L ratio from *c.* 0.56 in A-4 juveniles to *c.* 0.49 in the adult stage, which has a more elongated carapace shape. Small pustule-like elevations are visible on the surface of one specimen from the Early Triassic *Claraia* Beds (Fig. 8AB); these so-called ‘shell pustules’ were also observed on *Bairdiacypris ottomanensis* specimens from our study material and on material from the Zal section (Mette 2008, 2010; see remarks in the description of *B. ottomanensis* below).

Occurrence. Çürük dağ, Western Taurus, Turkey, Griesbachian (Crasquin-Soleau et al. 2004b; Forel 2014); Aras Valley, north-west Iran, *Claraia* Beds (Griesbachian), from $+2.88$ to $+6.05$ m (Fig. 4).

FIG. 9. Length/height scatter plot of *Araxobairdia formosa* Gliwa, sp. nov. from the Aras Valley section. Displayed specimens from left to right: AVn040-80, AVn040-111, ECO108. Scale bar represents 100 μ m.



Genus BAIRDIACYPRIS Bradfield, 1935

Type species. *Bairdiacypris deloi* Bradfield, 1935 by original designation.

Bairdiacypris ottomanensis Crasquin-Soleau in Crasquin-Soleau *et al.*, 2004b
Figures 10F–P, 12

- 2004b *Bairdiacypris ottomanensis* Crasquin-Soleau in Crasquin-Soleau *et al.*, p. 285, pl. 2, figs 13–24.
2014 *Praezabythocypris? ottomanensis* (Crasquin-Soleau); Forel, p. 11, text-fig. 8F–H. (for more synonymy)
2015 *Praezabythocypris? cf. ottomanensis* (Crasquin-Soleau); Forel *et al.*, p. 11, text-figs 5AG–AJ, p. 13, text-figs 7A–B.
2019 *Bairdiacypris ottomanensis* Crasquin-Soleau; Wan *et al.*, p. 8, text-fig. 4.2.

Material. 964 complete carapaces (L = 216–1014 μm ; Fig. 12).

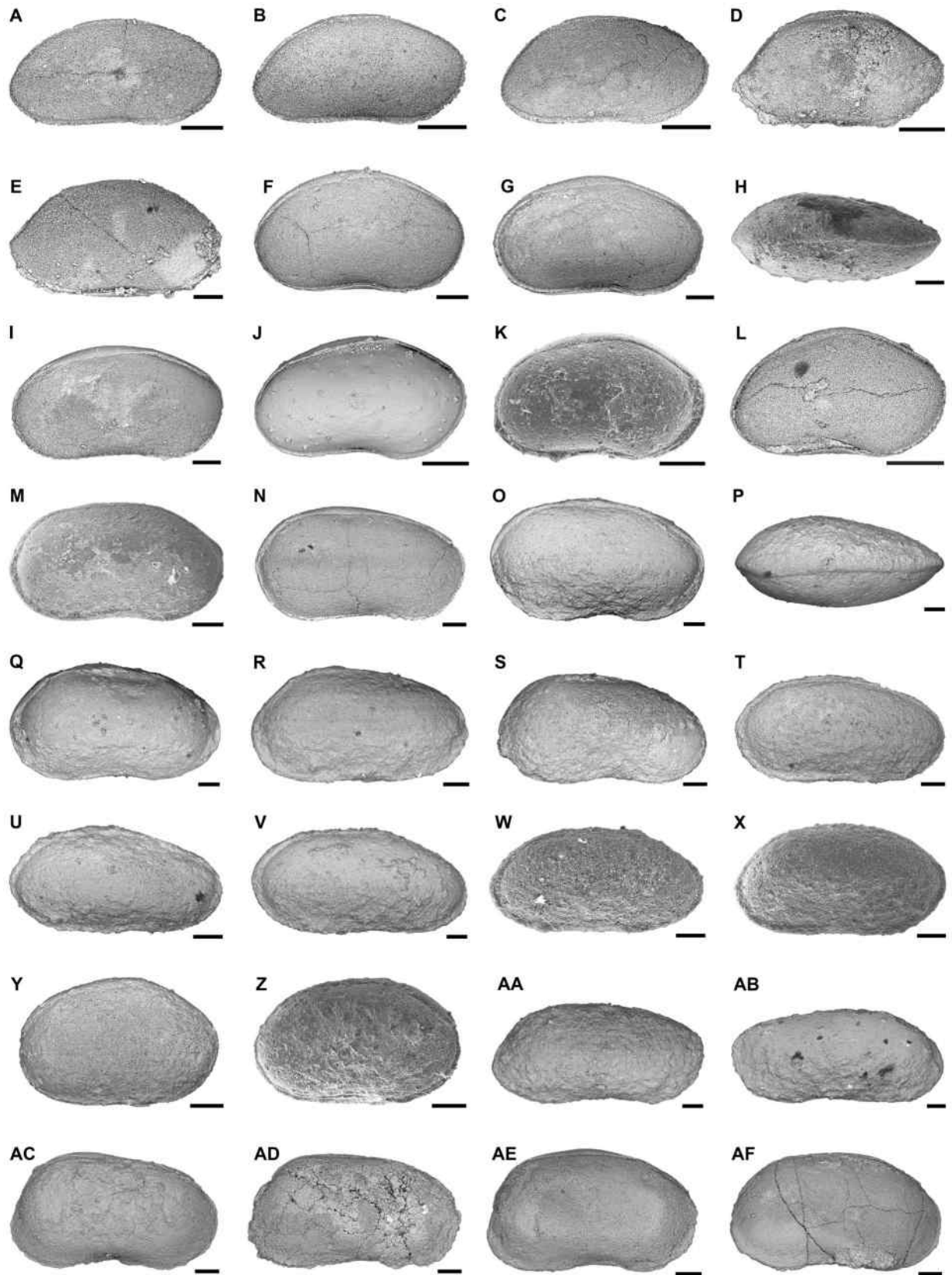
Remarks. The species was originally attributed to *Bairdiacypris* but included in *Praezabythocypris* by Mette (2010). In the genus description by Kozur (1985), the differentiation between *Bairdiacypris* and *Praezabythocypris* is based on a larger overlap of the left valve in *Praezabythocypris* and different muscle scar patterns, which are neither visible nor mentioned in the material described by Mette (2010) and also not illustrated by Kozur (1985). The lateral outline of the carapace and the angulate dorsal margin are characteristic for *Bairdiacypris*. Therefore, we follow the original attribution of the species to the genus *Bairdiacypris*. The specimen identified as *B. ottomanensis* by Liu *et al.* (2010) is excluded from this species because it shows no species-specific angulations in the dorsal margin.

As mentioned by Crasquin-Soleau *et al.* (2004b), there is a conspicuous intraspecific variation within *B. ottomanensis*, noticeable in a varying slope of the DB. In our material, smaller specimens have a more steeply sloping DB and a more narrowly rounded posterior margin with a maximum of convexity located in the lower third of H_{max} (Figs 10J–L, 12). In contrast, larger

specimens (identified as adults and A-1 instars) have a straight to slightly anteriorly/posteriorly tilted DB and a more rounded and higher posterior maximum of convexity (Fig. 10F–I, M–O). This may indicate ontogenetic development towards a slightly posteriorly tilted or straight to slightly anteriorly tilted DB and a widely rounded posterior margin with a higher maximum of convexity in the adult specimens. This morphological transition was partially recognized by Forel (2014) and is also recognized in some modern Bairdioidea, such as *Neonesidea oligodentata* (Kajiyama, 1913) (Smith & Kamiya 2002).

The specimens of our material can be divided in two morphotypes (Fig. 12): morphotype A, specimens with maximum of convexity in the lower third of H_{max} (in A-5 to A-3) or slightly below mid- H_{max} (in A-3 to adults) and DB distinctly or slightly posteriorly tilted (Fig. 10F–M); and morphotype B, specimens with a posterior widening and a slightly anteriorly tilted DB, with the maximum of height located more posteriorly (Fig. 10N–P). Morphotype A is present in all ontogenetic stages (A-5 to adults), whereas morphotype B starts in A-1 and is also present in the adult stage, where it represents the largest specimens (Fig. 12). These two morphotypes are interpreted here to represent sexual dimorphism. The division into the different morphotypes becomes visible in the A-1 stage of our material, where morphotype B starts to develop. Sexual dimorphism features on the carapace of some recent taxa are also known to become visible during A-1, for example, in *Uncinocythere occidentalis* (Smith & Kamiya 2005). In general, sexual dimorphism in *B. ottomanensis* is indicated by an inflated posterior part of the carapace in female specimens (Crasquin-Soleau *et al.* 2004b). Sexual dimorphism in the Podocopida is known from several modern and fossil examples, which show that male specimens are generally smaller; the posterior part of the female carapace, which contains the brood pouch, is usually inflated (Jaanusson 1985; Tanaka & Ikeya 2002; Smith & Hiruta 2004; Sato & Kamiya 2007; Tanaka & Seto 2010; Ozawa 2013; Forel *et al.* 2019). In our material, the specimens of morphotype B show a posterior widening and a slightly anteriorly tilted DB, with the maximum of height located more posteriorly (Fig. 10N–P). This posterior widening may be caused by the development of a brood pouch. Furthermore, morphotype B specimens are generally larger. We, therefore, interpret morphotype B as representing female specimens.

FIG. 10. SEM micrographs of ostracods from the Aras Valley section, north-west Iran. A–C, *Bairdia? kemerensis* Crasquin-Soleau, 2004: A, AV450X-72, right lateral view; B, AV450X-110, right lateral view; C, AV450X-05, right lateral view. D–E, *Bairdia* sp. 5: D, AV700-29, right lateral view; E, AV700-37, right lateral view. F–P, *Bairdiacypris ottomanensis* Crasquin-Soleau, 2004: F, AV450X-99, morphotype B, right lateral view; G, AV310-86, morphotype B, right lateral view; H, AV255SH-03, morphotype B, dorsal view; I, AV310-99, morphotype B, right lateral view; J, AV227-60, right lateral view; K, AV171SH-30, right lateral view; L, AV605-110, right lateral view; M, AV171SH-02, right lateral view; N, AV310-87, morphotype A, right lateral view; O–P, AV125SH-09, morphotype A: O, right lateral view; P, dorsal view. Q–S, *Bairdiacypris* sp. 1: Q, AV260-14, right lateral view; R, AV088X-39, right lateral view; S, AV075SH-14, right lateral view. T–V, *Bairdiacypris* sp. 2: T, AV116XSH-07, right lateral view; U, AV116XSH-42, right lateral view; V, AV265SH-92, right lateral view. W–X, *Bairdiacypris* sp. 3: W, AV116SH-66, right lateral view; X, AV116SH-74, right lateral view. Y–Z, *Bairdiacypris* sp. 4: Y, AV195TE-53, right lateral view; Z, AV152FO-23, right lateral view. AA–AB, *Bairdiacypris cf. longirobusta* Chen, 1958: AA, AV265SH-56, right lateral view; AB, AV288SH-158, left lateral view. AC–AF, *Bairdiacypris zaliensis* Mette, 2010: AC, AV227-31, right lateral view; AD, AV227-34, right lateral view; AE, AV227-18, right lateral view; AF, AV227-19, right lateral view. Scale bars represent 100 μm .



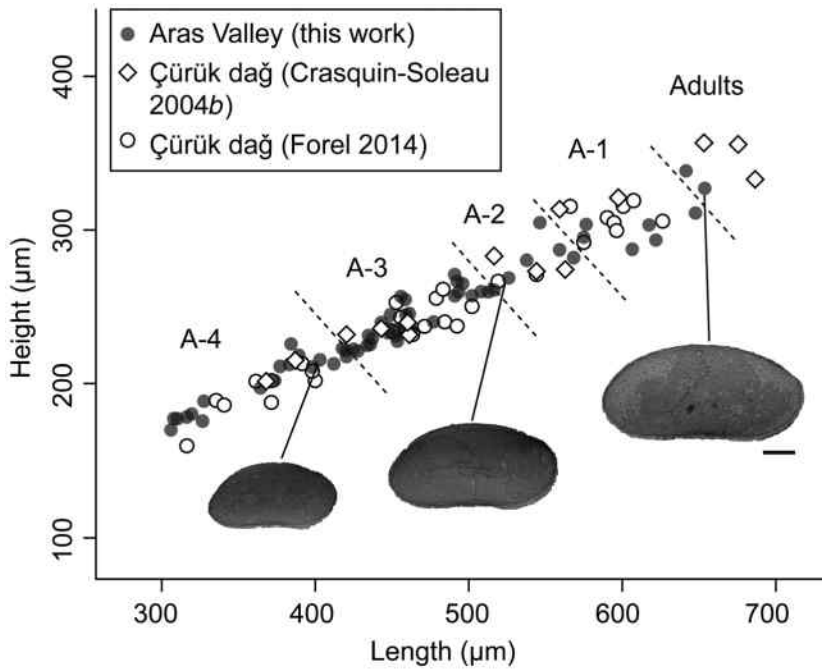


FIG. 11. Length/height scatter plot comparing *Bairdia? kemerensis* Crasquin-Soleau, 2004 from the Aras Valley section with the specimens described by Crasquin-Soleau *et al.* (2004b) and (Forel 2014) from Çürük dağ, Western Taurus, Turkey. Displayed specimens from left to right: AV450-08, AV450-67, AV310-36. Scale bar represents 100 μm .

Some specimens show a pustular shell surface (Fig. 10J), which was already mentioned by Mette (2008, 2010) in material from Zal. In these studies, the pustules were interpreted to be caused by environmental deterioration and changes in water chemistry. However, in our material, the specimens with pustules are clearly preserved as steinkerns and the pustules may correspond to filled pore channels. This interpretation is further supported by the occurrence of pustules in other specimens

from various species (*Liuzhinia antalyaensis* and *Bairdia? kemerensis*) in our material, which are also preserved as steinkerns.

Occurrence. Çürük dağ, Western Taurus, Turkey, Griesbachian (Crasquin-Soleau *et al.* 2004b; Forel 2014); Laolongdong section, Sichuan, South China, Griesbachian (Crasquin-Soleau & Kershaw 2005); Dajiang, Guizhou, South China, Griesbachian (Forel *et al.* 2009; Forel 2012); Elikah River, Central Alborz Mountains,

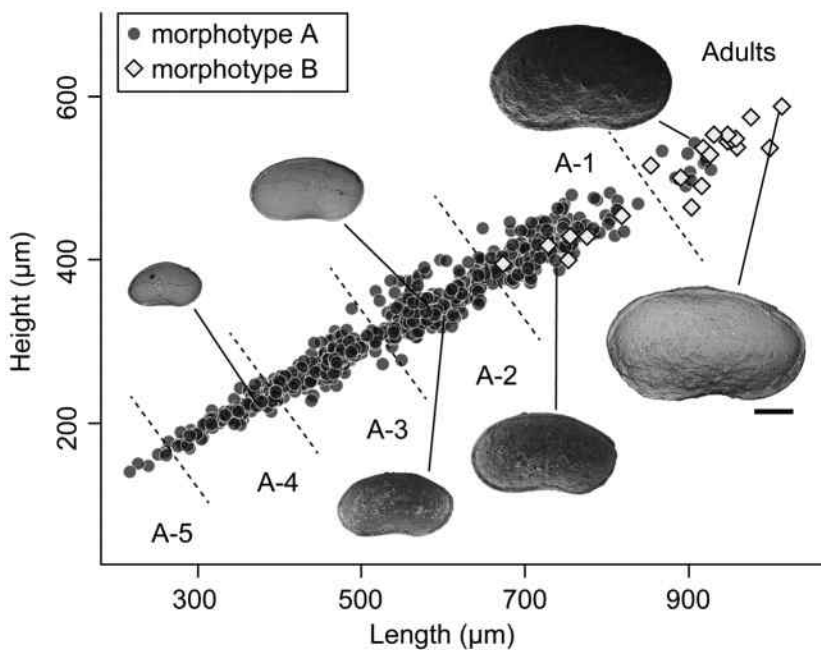


FIG. 12. Length/height scatter plot of *Bairdiacypris ottomanensis* Crasquin-Soleau, 2004 from the Aras Valley section. Displayed specimens from left to right: upper row, AV605-110, AV310-115, AV088TE-02; lower row, AV171SH-02, AV255SH-03, AV125SH-09. Scale bar represents 200 μm .

northern Iran, Changhsingian–Griesbachian (Forel *et al.* 2015); Zal, north-west Iran, Changhsingian–Griesbachian (Mette 2008, 2010); Aras Valley, north-west Iran, Aras Member and *Claraia* Beds (Changhsingian–Griesbachian), from +0.75 to +7.00 m (Fig. 4).

Bairdiacypris kathleenae Gliwa sp. nov.

Figures 13A–F, 14

LSID. urn:lsid:zoobank.org:act:68BFFDA7-3DA8-41F0-B1B3-2ED3DCF30A

Derivation of name. Named after Kathleen Schindler, who supported this work with her diligence and patience during the preparation of the material.

Type specimens. Holotype: complete carapace ECO110 (Fig. 13A, B), sample AV265. Paratype: complete carapace ECO111 (Fig. 13D), sample AV288.

Type locality and horizon. Aras Valley; *Claraia* Beds (Griesbachian), +2.65 m.

Material. 26 complete carapaces ($L = 811\text{--}1049\ \mu\text{m}$; Fig. 14).

Diagnosis. Species of *Bairdiacypris* with H_{max} located posterior to mid-L, large overlap of left valve all around the right valve and high posterior maximum of convexity.

Description. Carapace elongate, subreniform in lateral view with H_{max} in posterior half and L_{max} in the upper third of the carapace; oblong in dorsal view with slightly acuminate ends and largest width in the posterior third. Wide overlap of the larger left valve all around right valve, thinner along AVB. Dorsal margin nearly uniformly rounded at left valve and with very tenuous angulations in the right valve at the DB–PDB transition (*c.* 150°) located at the posterior third of L_{max} , and DB–PDB transition (*c.* 160°) slightly anterior to mid-L. Anterior end long, broadly rounded, truncate dorsally, with maximum of convexity approximately at mid-H. VB concave in right valve and straight to slightly concave in left valve. Posterior end broadly rounded with maximum of convexity slightly above mid-H. Surface smooth.

Remarks. The general outline and the wide overlap of the left valve in *B. kathleenae* are similar to the Lopingian *Fabalicypis visnyoensis* Kozur, 1985 from the Bükk Mountains in Hungary. However, the H/L ratio of *B. kathleenae* is generally higher and the posterior maximum of convexity is located above the medium height. Furthermore, there is no ventral offset of the overlapping left valve, which would indicate an affiliation to *Fabalicypis*.

In lateral view, the new species resembles the morphotype B specimens of *B. ottomanensis*, but the new species has a broader overlap. The difference between the two species is most

prominent in dorsal view; compared with *B. ottomanensis*, *B. kathleenae* possesses a more elongated carapace with nearly parallel valve outlines.

Occurrence. Aras Valley; Aras Member and *Claraia* Beds (Changhsingian–Griesbachian), from +1.52 to +3.75 m (Fig. 4).

Family INDET.

Genus EUMIRACULUM Chen *in* Shi & Chen, 1987

Type species. *Eumiraculum changxingensis* Chen *in* Shi & Chen, 1987 by original designation.

Eumiraculum mettei Gliwa sp. nov.

Figures 15Q–U, 16, 17

2008 *Microcheilinella* sp.; Mette, pl. 3, figs 5–7.

2010 *Microchelina* sp. 1; Mette, p. 30, pl. 4, figs 14–16.

LSID. urn:lsid:zoobank.org:act:26DC9D83-051B-4647-9F86-739111334D87

Derivation of name. Named after Wolfgang Mette, who first documented specimens of the new species from north-west Iran.

Type specimens. Holotype: complete carapace ECO112 (Fig. 15Q), sample AVn003. Paratype: complete carapace ECO113 (Fig. 15R), sample AVn140.

Type locality and horizon. Aras Valley; *Paratirolites* Limestone (Changhsingian), –0.03 m.

Material. 6 complete carapaces, 9 single valves ($L = 359\text{--}534\ \mu\text{m}$; Fig. 16) and 6 fragments.

Diagnosis. A species of *Eumiraculum* with subtriangular to drop-shaped carapace outline, two spines on the right valve and one spine on the left valve.

Description. Subtriangular to drop-shaped carapace outline in lateral view with L_{max} and H_{max} located close to the middle of the carapace; straight invaginated DB with lateral dorsomedial and mid-dorsal areas on both valves domed upwards, giving the DB a convexly rounded appearance in lateral view. Larger left valve overlaps right valve all around the carapace with maximum overlap at DB and VB, minimum at the posteroventral margin. Shallow lateral depression at the PB on both valves. Two small spines on right valve in posterodorsal and mid-posterior position (Fig. 17); one spine on dorsal margin of left valve, located in the posterior third and oriented slightly upward; this spine divides the outline of the dorsal margin in a concavely rounded posterior part and a convexly rounded anterior part, which merges uniformly to the AB. Uniformly and broadly rounded

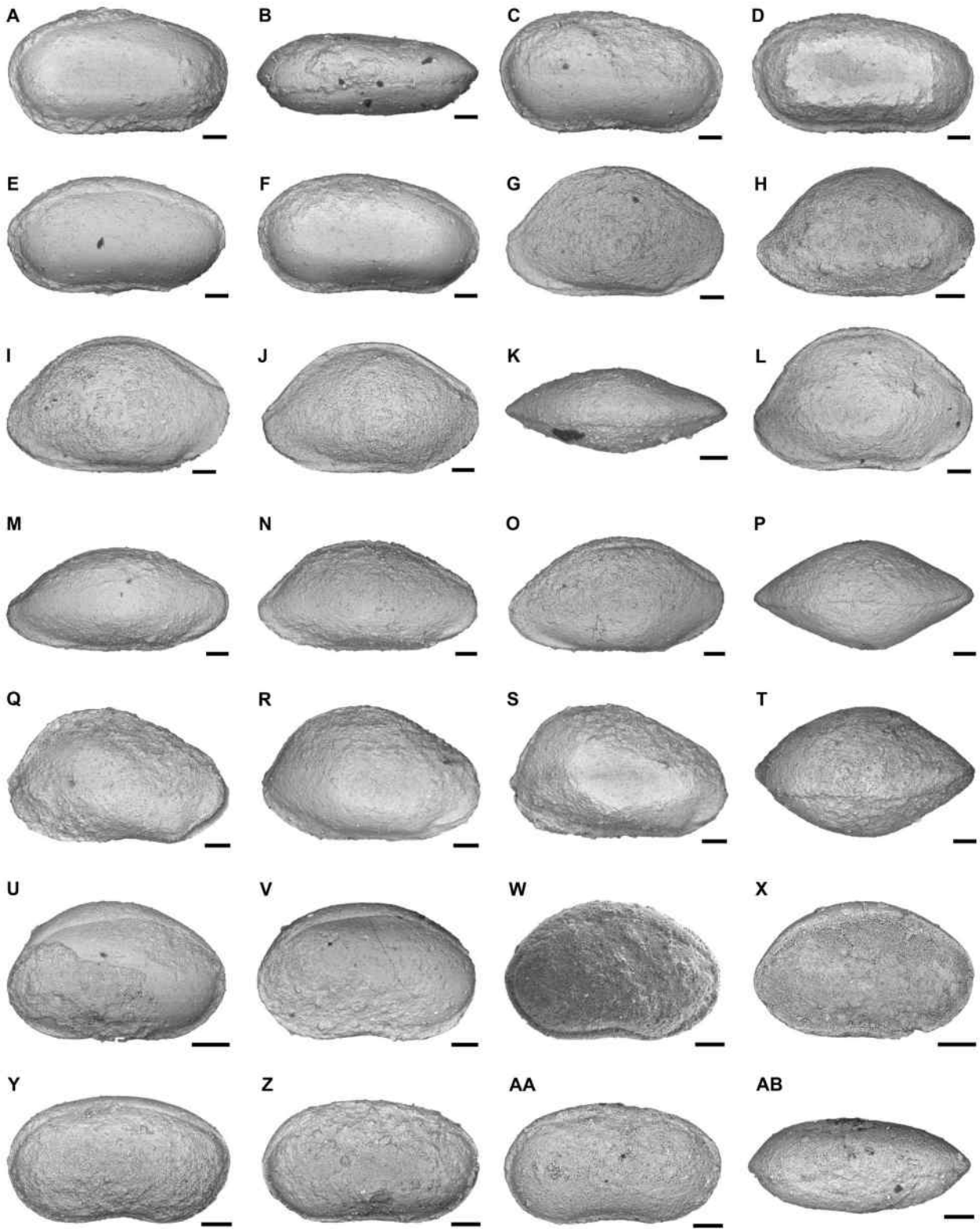
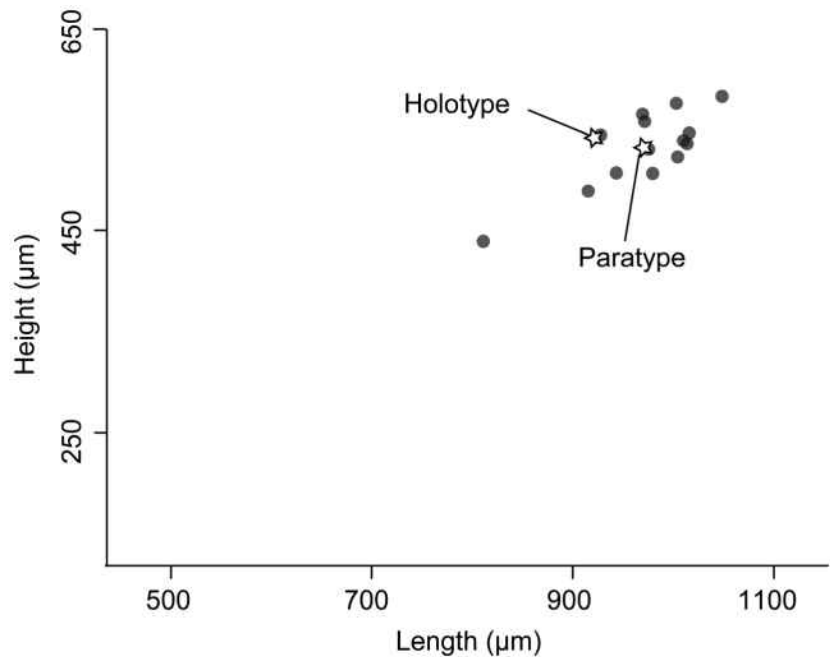


FIG. 13. SEM micrographs of ostracods from the Aras Valley section, north-west Iran. A–F, *Bairdiacypris kathleenae* Gliwa, sp. nov.: A–B, holotype ECO110: A, right lateral view; B, dorsal view; C, AV288SH-142, right lateral view; D, paratype ECO111, right lateral view; E, AV255SH-15, right lateral view; F, AV265SH-76, right lateral view. G–L, *Kempfina qinglaili* (Crasquin), 2008: G, AV015YTE-05, right lateral view; H, AV015XTE-19, right lateral view; I, AV005XTE-48, right lateral view; J, AV005XTE-25, right lateral view; K, AV015XTE-75, dorsal view; L, AV015YTE-99, right lateral view. M–P, *Kempfina* sp. 1: M, AV015YTE-36, right lateral view; N, AV005XTE-46, right lateral view; O, AV005XTE-54, right lateral view; P, AV015XTE-77, dorsal view. Q–T, *Kempfina* sp. 2: Q, AV015XTE-20, right lateral view; R, AV005X-05, right lateral view; S–T, AV015XTE-27: S, right lateral view; T, dorsal view. U–X, *Praezabythocypris* cf. *pulchra* sensu Forel, 2014: U, AV088X-22, right lateral view; V, AV152FO-129, right lateral view; W, AV088SH-05, right lateral view; X, AV088-209, right lateral view. Y–AB, *Praezabythocypris pulchra* Kozur, 1985: Y, AV185TE-07, right lateral view; Z, AV185TE-10, right lateral view; AA–AB, AV185SH-63: AA, right lateral view; AB, dorsal view. Scale bars represent 100 μm .

FIG. 14. Length/height scatter plot of *Bairdiacypris kathleenae* Gliwa, sp. nov. from the Aras Valley section.



AB. Transition between PB and VB gently angled at both valves (c. 125°). VB and PB uniformly curved. Posterior end with maximum of convexity located very high, in posterodorsal position. Carapace surface smooth.

Remarks. The new species resembles the Changhsingian material described as ‘*Eumiraculum desmaresae*’ by Forel *et al.* (2015) from the Central Alborz Mountains in Iran in its general outline of both valves in lateral view. However, the illustrated specimens of ‘*E. desmaresae*’ do not show any spines on the shell surface. The outline of *E. mettei* is also similar to the Lopingian *E. desmaresae* Forel in Forel *et al.*, 2013 from the Bükk Mountains in Hungary. In this species, the right valve overlaps the left valve at the AB and the anterior cardinal angle is underlain by a spine, which is not the case in the newly described species. *E. mettei* differs from the Lopingian *E. changxingensis* Chen in Shi & Chen (1987) from South China in its cardinal angles, which are located not higher than the dorsal margin but on the same height; and by its lateral surface, which is not marked by a longitudinal groove. In lateral view, the carapace shape of the new species is very close

to the early Wuchiapingian *Microcheilinella wujiapingensis* Zazzali in Zazzali *et al.* (2015) from Sichuan (China), but this is characterized by a smooth shell surface without spines.

Occurrence. Zal, north-west Iran, Wuchiapingian–Changhsingian (Mette 2008, 2010); Aras Valley, *Paratirolites* Limestone (Changhsingian), from –3.30 to –0.03 m (Fig. 4).

Genus LIUZHINIA Zheng, 1976

Type species. *Liuzhinia subovata* Zheng, 1976, by original designation.

Liuzhinia julfensis Gliwa sp. nov.

Figures 15AA–AF, 18

2008 *Liuzhinia?* sp.1; Mette, p. 215, pl. 2, figs 15–17.

2010 *Liuzhinia* sp. 1; Mette, p. 31, pl. 4, figs 7–9.

LSID. urn:lsid:zoobank.org:act:1C927486-AAFC-4A81-BAE5-8A50C20DD791

Derivation of name. After the town Julfa (north-west Iran) near the type locality.

Type specimens. Holotype: complete carapace ECO114 (Fig. 15AF), sample AV467. Paratype: complete carapace ECO115 (Fig. 15AE), sample AV310.

Type locality and horizon. Aras Valley; *Claraia* Beds (Griesbachian), +3.10 m.

Material. 29 complete carapaces (L = 527–659 µm; Fig. 18).

Diagnosis. Species of *Liuzhinia* with subtrapezoidal carapace with H_{\max} located anteriorly to mid-L and very low position of maximum of convexity at the anterior and posterior ends.

Description. Subtrapezoidal, elongated outline in lateral view; H_{\max} located in the anterior third of L_{\max} . Very thin overlap of the larger left valve, particularly visible along the VB. Dorsal margin straight to slightly rounded with a gentle angulation between PDB and DB, located in the posterior fourth of L_{\max} . DB slightly convex, uniformly and broadly rounded to the AB. Anterior end rounded with large radius of curvature and maximum of convexity located in the lower fourth of H_{\max} . VB straight to very slightly concave. Posterior end more narrowly rounded with maximum of convexity located in the lower fourth of H_{\max} . Short, convex PDB bent towards the DB with an angle of 125–135°. Carapace surface smooth.

Remarks. The new species resembles the Griesbachian *L. antalyaensis* Crasquin-Soleau in Crasquin-Soleau *et al.*, 2004b in its general lateral outline, but *L. julfensis* is more elongate (lower H/L) with a lower H/L in the holotype of 0.48 compared with H/L = 0.57 in *L. antalyaensis*. Furthermore, the anterior maximum of convexity is located lower than in *L. antalyaensis*. The latest Permian *L. praeantalyaensis* Forel in Crasquin *et al.*, 2010 from Meishan (Crasquin *et al.* 2010) has a similar lateral outline but differs by its narrower posterior end and by its anterior

maximum of convexity located at mid-H. In contrast to the specimens figured by Mette (2008, 2010), the shell surface of our material is smooth without any pustules. These ‘pustulae’, described in Mette (2008, 2010) as an ‘ecophenotypic feature’ derive from its preservation as steinkern and are not specific features for the species.

Occurrence. Zal, north-west Iran, Griesbachian (Mette 2008, 2010); Aras Valley, Aras Member and *Claraia* Beds (Changhsingian–Griesbachian), from +1.71 to +4.67 m (Fig. 4).

Order PALAEOCOPIDA Henningsmoen, 1953
Suborder KIRKBYOCOPINA Gründel, 1969
Superfamily KIRKBYOIDEA Ulrich & Bassler, 1906
Family KIRKBYIDAE Ulrich & Bassler, 1906

Genus CARINAKNIGHTINA Sohn, 1970

Type species. *Carinaknightina carinata* Sohn, 1970, by original designation.

Carinaknightina hofmanni Gliwa sp. nov.
Figures 19O–V, 20

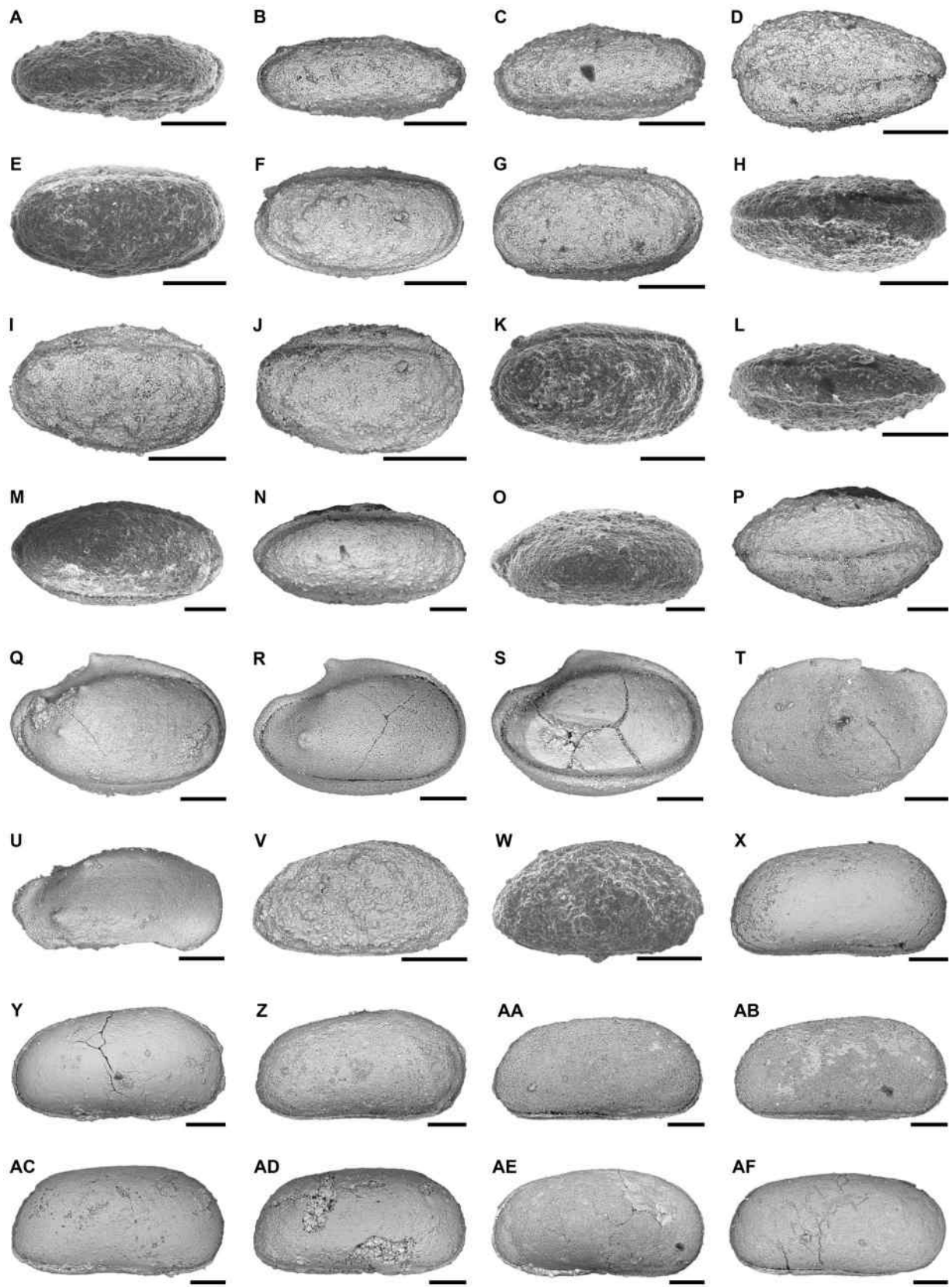
LSID. urn:lsid:zoobank.org:act:4334AE3B-8DD2-4900-86E6-8945CB176132

Derivation of name. Named after Richard Hofmann, for his scientific and good-humoured support.

Type specimens. Holotype: complete carapace ECO116 (Fig. 19O, P), sample AV028. Paratypes: complete carapace ECO117 (Fig. 19Q), sample AV028; complete carapace ECO118 (Fig. 19U, V), sample AV028.

Type locality and horizon. Aras Valley; Aras Member (Changhsingian), +0.28 m.

FIG. 15. SEM micrographs of ostracods from the Aras Valley section, north-west Iran. A–D, *Microcheilinella* cf. *perexilis* Shi in Shi & Chen, 1987: A, AV005TE-45, right lateral view; B, AV005XTE-18, right lateral view; C, AV005XTE-19, right lateral view; D, AV005TE-46, dorsal view. E–L, *Microcheilinella* sp. 1: E, AV005TE-24, right lateral view; F, AV015Z-24, right lateral view; G–H, AV005XTE-02: G, right lateral view; H, ventral view; I, AV015Z-02, right lateral view; J, AV015Z-42, right lateral view; K–L, AV005TE-27: K, right lateral view; L, dorsal view. M–P, *Microcheilinella* sp. 2: M, AV015TE-10, right lateral view; N, AV015TE-09, right lateral view; O, AV015TE-08, right lateral view; P, AV015TE-10, dorsal view. Q–U, *Eumiraculum mettei* Gliwa, sp. nov.: Q, holotype ECO112, right lateral view; R, paratype ECO113, right lateral view; S, AVn330-88, right lateral view; T, left valve, AVn40-84, left lateral view; U, right valve, AVn40-12, right lateral view. V–W, *Liuzhinia*? sp. 1: V, AV005X-17, right lateral view; W, AV005XTE-11, right lateral view. X–Z, *Liuzhinia antalyaensis* Crasquin-Soleau, 2004: X, AV227-25, right lateral view; Y, AV227-64, right lateral view; Z, AV260-66, right lateral view. AA–AF, *Liuzhinia julfensis* Gliwa, sp. nov.: AA, AV310-65, right lateral view; AB, AV310-34, right lateral view; AC, AV227-20, right lateral view; AD, AV227-16, right lateral view; AE, paratype ECO115, right lateral view; AF, holotype ECO114, right lateral view. Scale bars represent 100 µm.



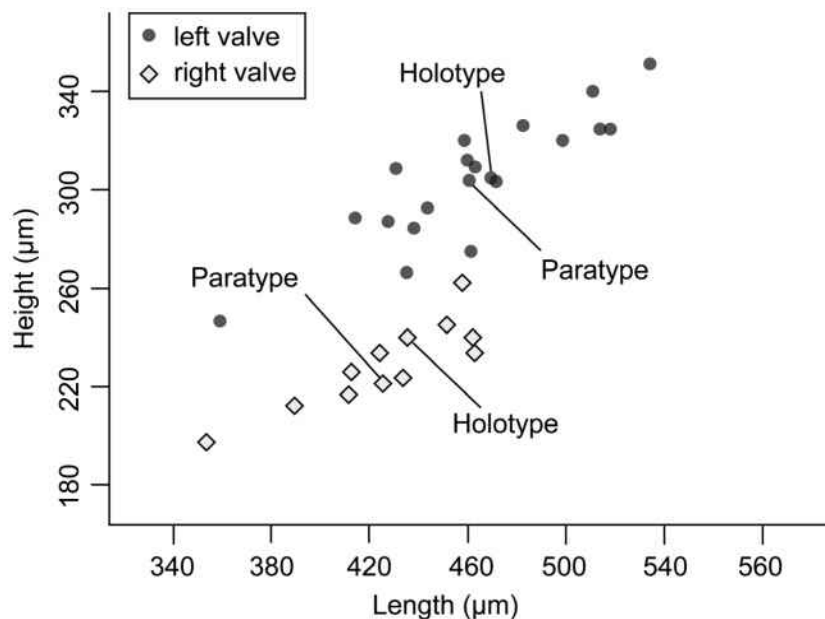


FIG. 16. Length/height scatter plot of *Eumiraculum mettei* Gliwa, sp. nov. from the Aras Valley section.

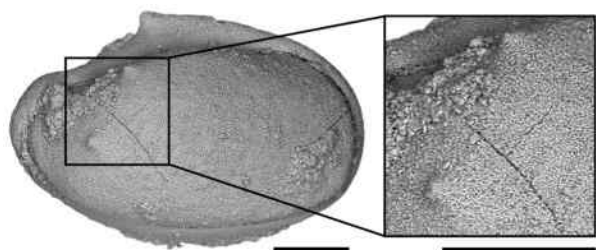


FIG. 17. Specimen of *Eumiraculum mettei* Gliwa, sp. nov. (holotype, ECO112) with magnified spines on the right valve. Scale bars represent 100 µm.

Material. 23 complete carapaces (L = 367–601 µm; Fig. 20).

Diagnosis. Species of *Carinaknightina* with subrectangular to subtriangular carapace, velate ridge running parallel to the marginal ridge. Two distinct lateral ridges extending from posterodorsal to mid-anterior area.

Description. Subrectangular to subtriangular carapace in lateral view; H_{max} located in the anterior third and L_{max} close to the middle of the carapace. Both valves approximately equal in size, no overlap visible. Long (70–75% of L_{max}), straight DB with dorsal ridge. Velate ridge, parallel to the marginal ridge, extending from below the anterior cardinal angle to below the posterior cardinal angle. AB rounded with maximum of convexity at the lower third of H_{max} . Straight to slightly concave VB. PB uniformly rounded. Anterior cardinal angle = 125–140°, posterior cardinal angle *c.* 120°. One major lateral ridge, extending from the posterodorsal to mid-anterior area, along the dorsomedian area and above a slightly oval pit at the median area, which is located slightly behind mid-length. Another, shallower and

shorter lateral ridge extends along the mid-dorsal area subparallel to the major lateral ridge. Intra-ridge areas are reticulate with relatively large reticules that have thick muri.

Remarks. The new species is similar, in its reticulate surface and lateral outline, to the Wuchiapingian *C. tricarinata* Kozur, 1985 from the Bükk Mountains in Hungary. However, *C. tricarinata* has a significantly shallower kirkbyan pit and a larger H/L ratio. Furthermore, the new species has only two distinct lateral ridges. The most ventral ridge in *C. tricarinata* is not present in *C. hoffmanni*.

Occurrence. Aras Valley; Aras Member (Changhsingian), +0.28 m (Fig. 4).

Order PLATYCOPIDA Sars, 1866
Suborder PLATYCOPINA Sars, 1866
Superfamily CAVELLINOIDEA Egorov, 1950
Family CAVELLINIDAE Egorov, 1950

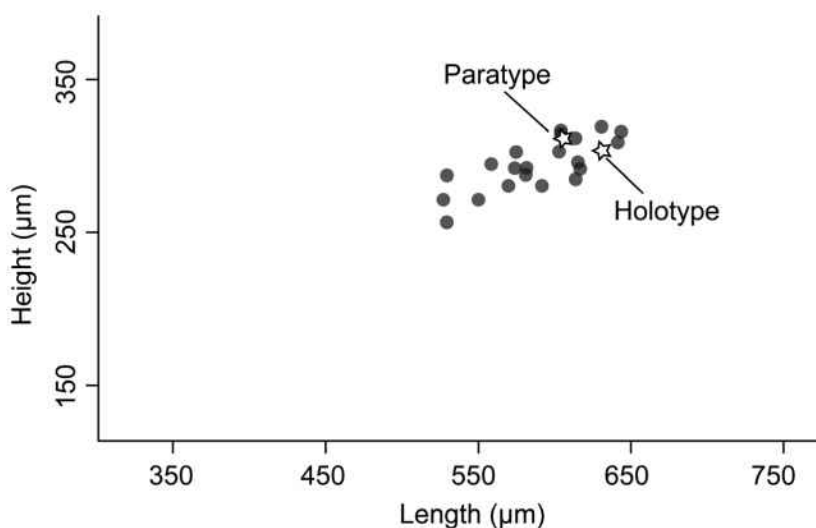
Genus CAVELLINA Coryell, 1928

Type species. *Cavellina pulchella* Coryell, 1928, by original designation.

Cavellina fosteri Gliwa sp. nov.
Figures 21J–W, 22

LSID. urn:lsid:zoobank.org:act:5408B079-A444-4DDF-87EE-B8E526F87FCB

FIG. 18. Length/height scatter plot of *Liuzhinia julfensis* Gliwa, sp. nov. from the Aras Valley section.



Derivation of name. Named after William J. Foster, who provided the authors with new ideas.

Type specimens. Holotype: complete carapace ECO119, morphotype A (Fig. 21T, U), sample AV028. Paratypes: complete carapace ECO120, morphotype B (Fig. 21L, M), sample AV075; complete carapace ECO121, morphotype A (Fig. 21R, S), sample AV028.

Type locality and horizon. Aras Valley; Aras Member (Changhsingian), +0.28 m.

Material. 109 complete carapaces (L = 277–635 µm; Fig. 22).

Diagnosis. Species of *Cavellina* with subrectangular (morphotype A) to subovate (morphotype B) carapace, broadly rounded anterior half and inflated posterior part (morphotype B); posteroventral area and anterior margin laterally compressed.

Description. The species shows two morphologies, marked as morphotype A and B: morphotype A (Fig. 21J–Q) is subrectangular in lateral view with H_{max} located in the anterior third of L_{max} . Right valve overlaps left valve all around the carapace with smallest overlap at AB and PB. Fusiform shape in dorsal view with tapered anterior and posterior ends and W_{max} (W/L c. 0.30) slightly posterior to mid-L. DB long (c. 65% of L_{max}), straight to slightly convex. PB broadly rounded, with angle between PB and DB c. 90°. VB slightly concave to straight. AB broadly, uniformly rounded, maximum of convexity slightly below mid-H. Posteroventral area and anterior margin laterally compressed. Shallow sulcus located in mid-dorsal area extending down to mid-H of the carapace. Carapace surface smooth.

Morphotype B (Fig. 21R–V) is subovate in lateral view with H_{max} in the middle third L_{max} . Wedge-shaped in dorsal view with bulbous posterior and tapered anterior part (W/L c. 0.40). Right valve larger than left valve, overlapping all around the carapace with maximum at DB. Posteroventral area and anterior margin

laterally compressed. Sulcus visible at mid-dorsal area. DB bent towards PB with an angle of 100–110°; PB uniformly and more narrowly rounded than AB. AB broadly rounded with maximum of convexity slightly below mid-H. VB straight to slightly concave, sometimes slightly convex. Dorsal margin in left valve slightly convex rounded, bent with an angle c. 150° between ADB and the nearly straight DB; dorsal margin in right valve convex and uniformly rounded, PB rounded with maximum of convexity located slightly above mid-H. Carapace surface smooth.

Remarks. The two morphotypes are interpreted to represent sexual dimorphs. Sexual shell dimorphism in platycopids and specifically in cavellinids is already well-known; it is induced by an enlargement of the domiciliary cavity in the most posterior part of the female specimens (heteromorphs) due to egg care (Jaanusson 1985). Morphotype B shows a bulbous, inflated posterior part, which is wedge-shaped in dorsal view (Fig. 21S, U), a character that is known in female carapaces of cavellinids. The carapace of morphotype A, which is interpreted to represent the male morphology of larger specimens (from A-1 stage), is more rectangular in overall shape as well as fusiform and slim in dorsal view (Fig. 21K, M). This dimorphism is expressed only in the adult and A-1 instar specimens.

Occurrence. Aras Valley; Aras Member (Changhsingian), from +0.28 to +1.52 m (Fig. 4).

Cavellina hairapetiani Gliwa sp. nov.
Figures 21X–AA, 23

LSID. urn:lsid:zoobank.org:act:DDEED02C-5616-4857-9114-8FA05C4D2492

Derivation of name. Named after Vachik Hairapetian, who supported the authors during field work in north-west Iran.

Type specimens. Holotype: complete carapace ECO122 (Fig. 21X, Y), sample AV125. Paratype: complete carapace ECO123 (Fig. 21Z, AA), sample AV116.

Type locality and horizon. Aras Valley; Aras Member (Changhsingian), +1.25 m.

Material. 9 complete carapaces (L = 484–529 μm ; Fig. 23).

Diagnosis. Species of *Cavellina* with a high H/L ratio and a short subcircular to oval carapace in lateral view; in dorsal view wedge-shaped with a strongly inflated posterior part.

Description. Short, subcircular to oval carapace in lateral view. H_{max} located in the middle or slightly posterior to it, L_{max} located around mid-H. In dorsal view wedge-shaped with large width (W/L c. 0.5) and asymmetrical posterior part with wider right valve. W_{max} distributed around the posterior half of the carapace. Right valve overlaps smaller left valve at dorsal and ventral margin in lateral view. At PB, left valve slightly longer than right valve, no overlap visible. Dorsal margin uniformly rounded. Posterior part of left valve strongly inflated; PB rounded with smaller radius of curvature than in AB; maximum of convexity located at the upper third of H_{max} . Straight to convex VB. AB rounded with maximum of convexity in the lower half of H. ADB straight to slightly convex, gently bent towards the straight-to-convex PDB (c. 155°). AB tapered. Very shallow sulcus visible in the anterodorsal area. Surface smooth.

Remarks. The largest specimens of *C. hairapetiani* have usually a more elongate carapace compared with the smaller ones. It is unclear which growth stage the large specimens belong to, given that the L/H diagram shows one uniform scatter without distinct stage boundaries (Fig. 23). All 14 specimens possess a strongly inflated posterior part, which may indicate an attribution to female representatives (Jaanusson 1985) of all recovered specimens. It is not clear from the material whether the new species is generally characterized by this posterior enlargement of the carapace or if male representatives have not been discovered yet.

The new species slightly resembles, in its general short and roundish lateral outline, the Changhsingian *C. alpina* Crasquin *in Crasquin et al.* (2008) from the Dolomites. In dorsal view, however, there is no inflation of the posterior part visible in *C. hairapetiani*. Furthermore, the dorsal margin of *C. alpina* is

marked by a pronounced angulation around mid-L, while the dorsal margin is uniformly rounded in *C. hairapetiani*.

Occurrence. Aras Valley; Aras Member (Changhsingian), from +0.28 to +1.25 m (Fig. 4).

Subclass MYODOCOPA Sars, 1866
Order MYODOCOPIDA Sars, 1866
Suborder MYODOCOPINA Sars, 1866
Superfamily CYLINDROLEBERIDOIDEA Müller, 1906
Family CYLINDROLEBERIDIDAE Müller, 1906

Genus HUNGAROLEBERIS Tóth & Cséfan, 2018

Type species. *Hungaroleberis retiferus* Tóth & Cséfan, 2018 by original designation.

Hungaroleberis striatus Forel sp. nov.
Figures 24V–AB, 25, 26

LSID. urn:lsid:zoobank.org:act:FB8A5EFB-677E-455D-B4B6-EB3B02F621F5

Derivation of name. From the Latin *striatus*, striate, referring to the ornamentation.

Type specimens. Holotype: complete carapace ECO124 (Fig. 24V), sample AVn330. Paratype: complete carapace ECO125 (Fig. 24W), sample AVn330.

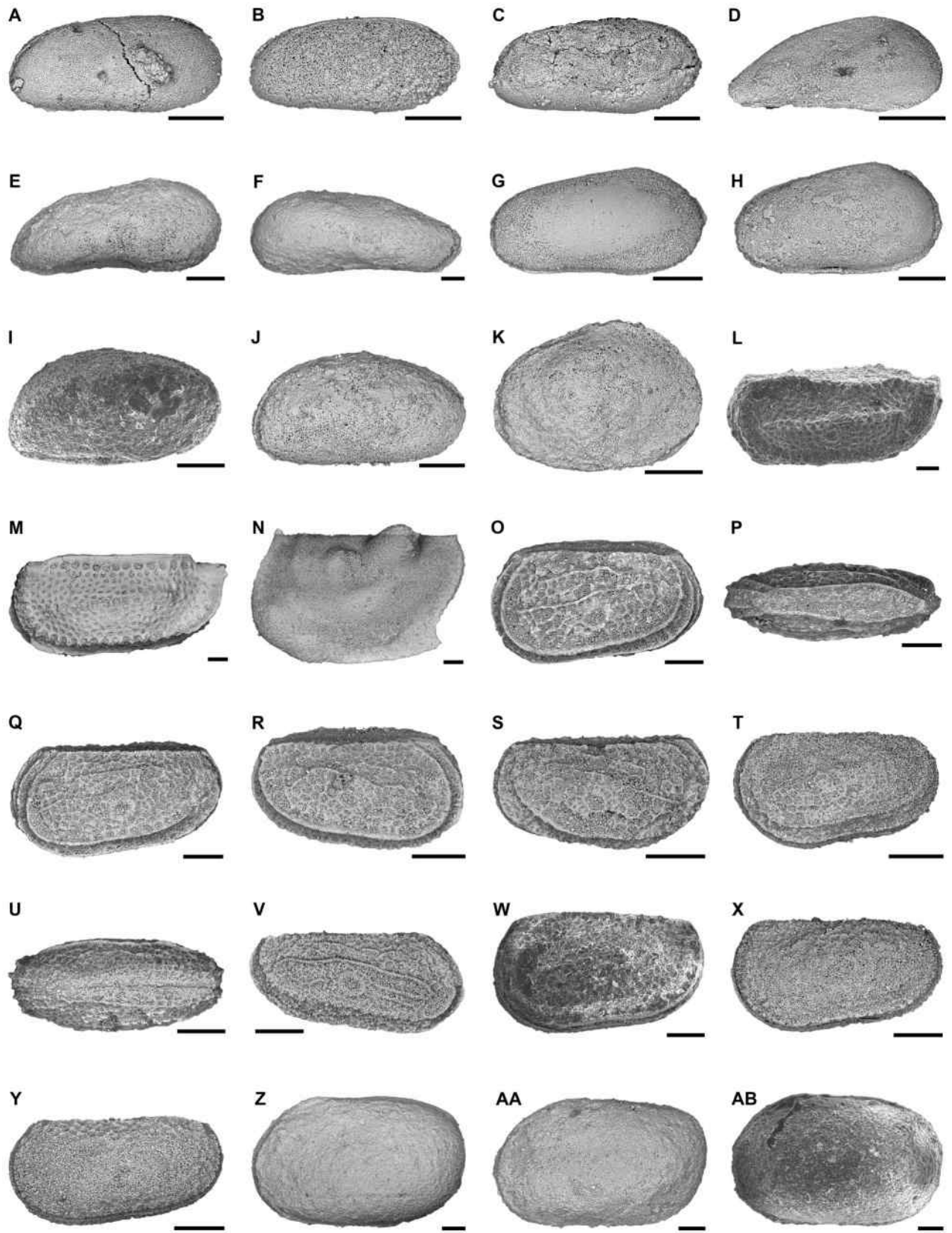
Type locality and horizon. Aras Valley; *Paratirolites* Limestone (Changhsingian), –3.30 m.

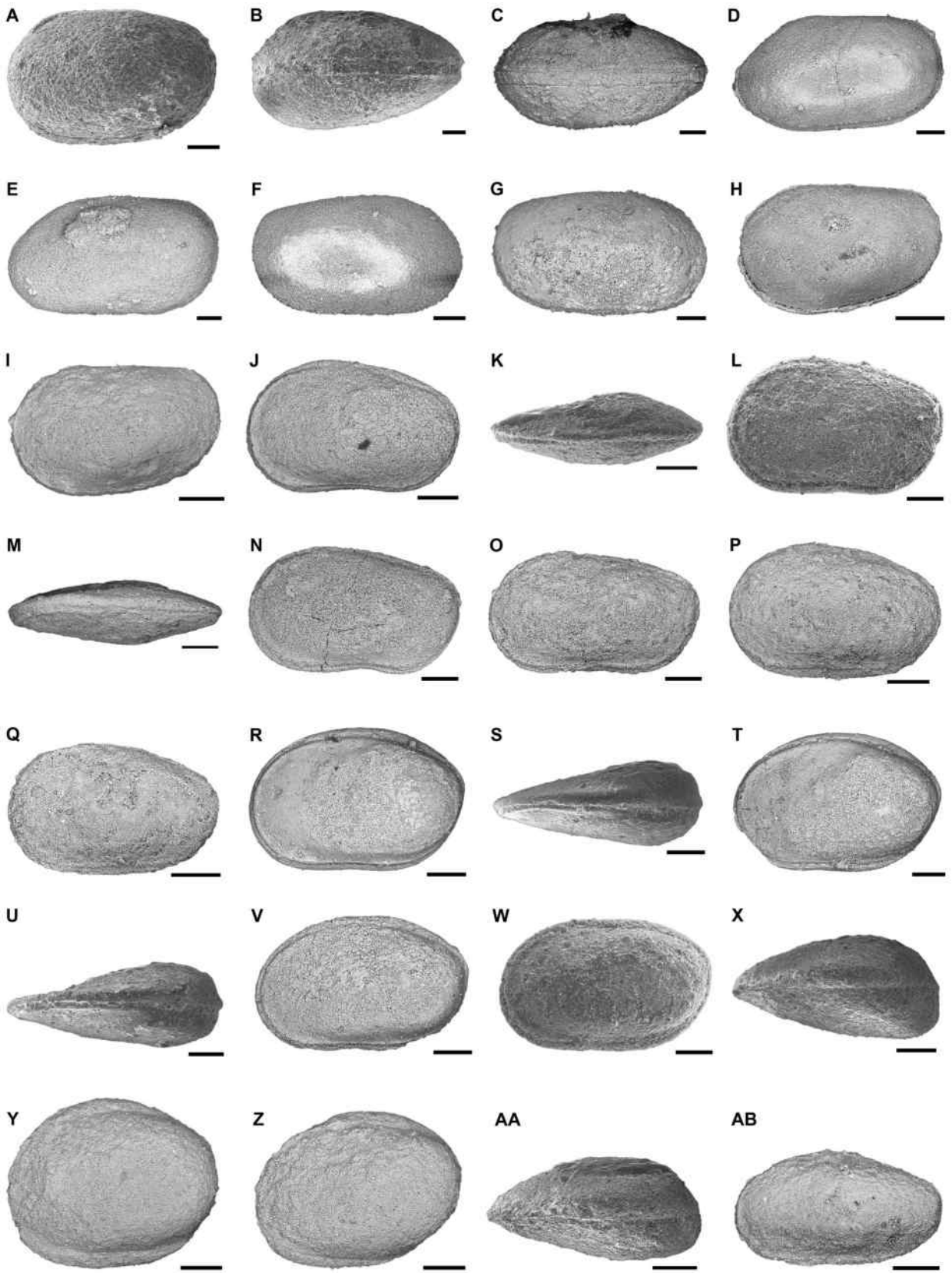
Material. 73 complete carapaces (L = 309–740 μm ; Fig. 25).

Diagnosis. Species of *Hungaroleberis* with striate surface.

Description. Carapace of medium size, ovoid to subquadrate in lateral view, with H_{max} at AD angulation and L_{max} at tip of

FIG. 19. SEM micrographs of ostracods from the Aras Valley section, north-west Iran. A–C, *Liuzhinia* sp. 2: A, AV700-17, right lateral view; B, AV700-20, right lateral view; C, AV700-28, right lateral view. D, *Paracypris* sp. 1, AVn040-40, right lateral view. E–F, *Paracypris* sp. 2: E, AV088-104, right lateral view; F, AV060TE-21, left lateral view. G–H, *Paracypris gaetanii* Crasquin-Soleau *in Crasquin-Soleau et al.*, 2006a: G, AV227-66, right lateral view; H, AV227-63, right lateral view. I–J, *Hungarella* sp. 1: I, AV028YSH-27, right lateral view; J, AV015XTE-53, right lateral view. K, *Basslerella* sp. 1, AV028YTE-52, right lateral view. L–M, *Iranokirkbya brandneri* Kozur & Mette, 2006: L, AV005TE-07, left lateral view; M, AV005TE-51, left lateral view. N, *Hollinella* sp. 1, left valve, AVn040-101, left lateral view. O–V, *Carinaknightina hofmanni* Gliwa, sp. nov.: O–P, holotype ECO116: O, left lateral view; P, dorsal view; Q, paratype ECO117, left lateral view; R, AV028YTE-06, right lateral view; S, AV028YTE-55, right lateral view; T, AV028YTE-43, left lateral view; U–V, paratype ECO118: U, dorsal view; V, right lateral view. W–Y, *Reviya* sp. 1: W, AV028TE-10, left lateral view; X, AV028YTE-87, left lateral view; Y, AV028YTE-14, left lateral view. Z–AB, *Buregia?* sp. 1: Z, AV185SH-42, left lateral view; AA, AV260-23, left lateral view; AB, AV171SH-62, left lateral view. Scale bars represent 100 μm .





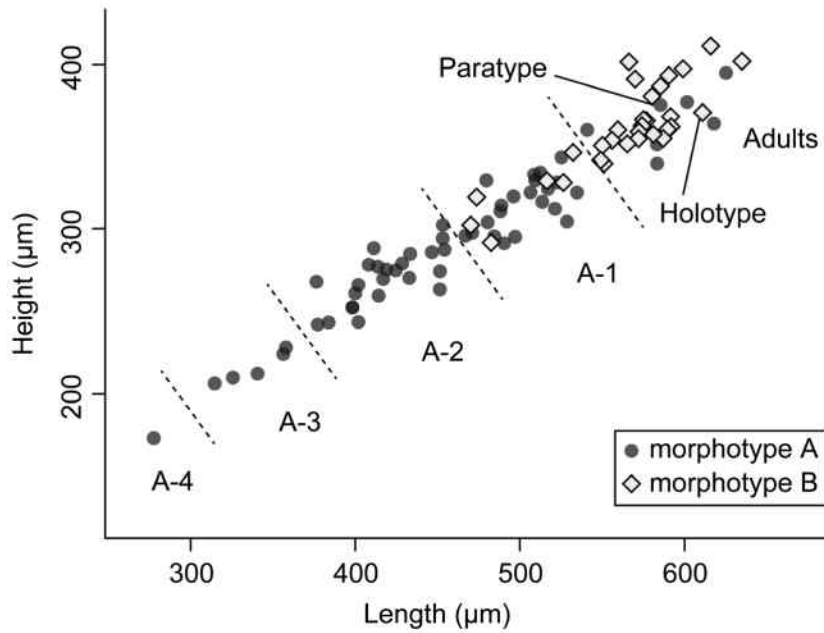


FIG. 22. Length/height scatter plot of *Cavellina fosteri* Gliwa, sp. nov. from the Aras Valley section.

(Crasquin-Soleau & Baud 1998) to Bajocian (Tóth & Cséfan 2018) strata. In terms of palaeogeographical distribution, Guadalupian occurrences of *Hungaroleberis* are known only from Greece (Crasquin-Soleau & Baud 1998); the genus is more widely distributed in Lopingian rocks, e.g. Greece (Crasquin-Soleau & Baud 1998), South China (Crasquin *et al.* 2010) and Iran (this work). According to current knowledge, Middle and Late Jurassic occurrences of *Hungaroleberis* are restricted to Hungary (Tóth & Cséfan 2018).

Occurrence. Aras Valley; *Paratirolites* Limestone (Changhsingian), -3.30 to -1.40 m (Fig. 4).

RESULTS

For the present study with a focus on the EPME, 59 samples from the Aras Valley section (north-west Iran) were investigated for their ostracod content. The ostracod abundances of the samples ranged from 4 to 31 500 specimens per 500 g. In total, 3425 specimens were identified to the species level with 62 species belonging to 23 genera and 12 families (Fig. 4; see Tables 1–3 for a list of all identified species and Gliwa *et al.* 2020b, table S1 for specimen occurrences per species and sample horizon).

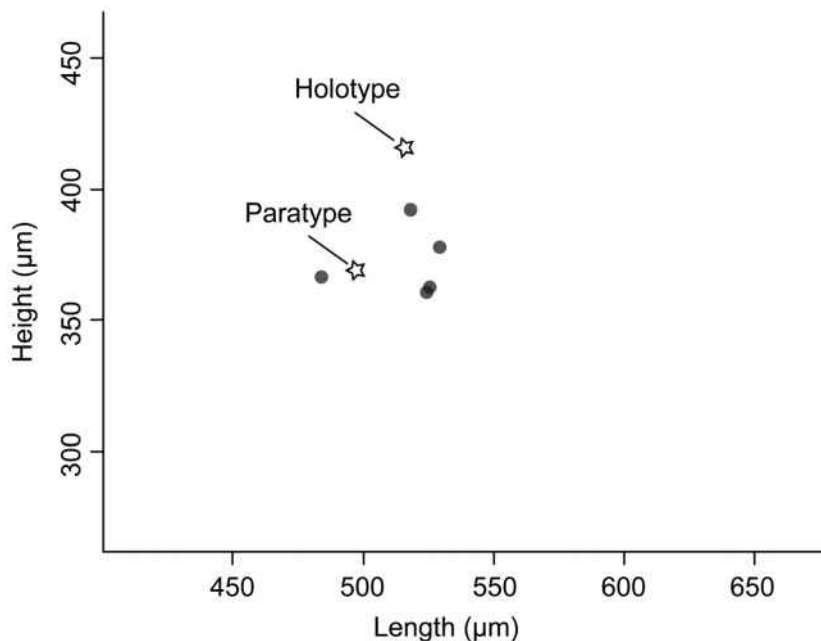


FIG. 23. Length/height scatter plot of *Cavellina hairapetiani* Gliwa, sp. nov. from the Aras Valley section.

Ten species and one genus are described here for the first time. 36 species are kept in open nomenclature because of poor preservation of the specimens.

Length/height diagrams show that for most of the studied species, the values of ontogenetic stages plot in distinct clusters. As Boomer *et al.* (2003) showed for other occurrences, such a distribution in which several juvenile stages as well as the adult stage are represented in the samples, indicates the absence of a strong energetic sorting process due to transportation over long distances. Furthermore, the usually complete preservation of carapaces lets us assume that the specimens represent autochthonous material (Brouwers 1988). The abundance, diversity and taxonomic patterns within the three lithological units of the studied interval show the following characteristics.

1. *Paratirolites* Limestone: the abundance of ostracods in this pre-extinction interval ranges usually between 200 and 300 specimens but reaches 600–700 in the horizons at –3.30 m, –0.40 m and –0.03 m (Fig. 27). The species diversity is generally low with 3–8 species per sample (Fig. 27). A monospecific assemblage occurs at –0.01 m in the topmost horizon of the *Paratirolites* Limestone; this exclusively contains the species *Fabalicypriis obunca*.

The ostracod assemblages within the *Paratirolites* Limestone are mainly composed of species of the order Podocopida, of which the species *Fabalicypriis obunca* is predominant. The only exception occurs in the interval from –3.30 to –1.40 m, which is marked by abundant occurrences of *Hungaroleberis striatus*, the only myodocopid species in the studied section. Up to 43% of the total specimens consists of this possibly nektonic/planktonic ostracod species (Fig. 27).

2. Aras Member: the abundance of ostracods in the samples is very heterogeneous and ranges from 6 to 31 500 per 500 g material. The samples between +0.45 and +0.75 m and at +1.25 m are marked by very low numbers (6–46 specimens), while sample +1.71 m contains ostracod mass occurrences c. 31 500 specimens per 500 g material. The diversity increases within the Aras Member; it reaches a maximum of 16 species at +1.16 m but subsequently drops to four species at +1.71 m. This first diversity increase in the lower part of the Aras Member is paralleled by a complete faunal turnover (Fig. 4). The poorly diverse *Fabalicypriis*-dominated ostracod assemblage from the *Paratirolites* Limestone was replaced by a relatively diverse *Bairdiacypris*-dominated assemblage. The assemblage in the Aras Member is dominated by podocopid species but the occurrences of platycopid and palaeocopid species show that diversity increases also on a higher taxonomic level (Fig. 27).

3. *Claraia* Beds: the abundance of ostracods in the lower 0.70 m of the *Claraia* Beds is relatively high, ranging from 1000 to 2500 specimens per 500 g sample material, with occasional very low numbers (down to four specimens) in the upper part of the sampled interval (+3.20 m to +7.00 m). A peak of diversity (15 species) occurs at +2.65 m and is immediately followed by low species numbers (between two and five in samples +3.10 to +6.05 m). Up to the sample at +6.05 m, the assemblages are dominated by *Bairdiacypris ottomanensis*. In the uppermost sample (+7.00 m), the taxonomic composition changes to a *Bairdia*-dominated assemblage together with occurrences of *Liuzhinia* sp. 2 and only one specimen of *B. ottomanensis*. All assemblages in the *Claraia* Beds are dominated by podocopid species. The only occurrences of Palaeocopida and Platycopida in the lower part are paralleled by the short diversity peak at +2.65 m (Fig. 27).

DISCUSSION

Palaeoenvironmental setting

With the occurrence of the Bairdiidae, Palaeocopida and Cavellinidae, the ostracod assemblages of the Aras Valley section show a characteristic genus composition, typically found in tropical marine environments (Crasquin-Soleau *et al.* 2004a). Following the interpretations of Peterson & Kaesler (1980), Melnyk & Maddocks (1988) and Costanzo & Kaesler (1987), some genera, families and superfamilies have distinct characteristics with regard to their environment: (1) Bairdiidae are present in deep to shallow environments with normal marine salinity; (2) *Microcheilinella*, *Basslerella* and Kirkbyidae are instead distributed in environments with normal salinity and oxygenation on the distal platform; (3) Cavellinidae occur in shallow (large, robust forms) but also in relatively deeper settings on the intermediate zone of the platform (small forms); the diversity of cavellinids increases in shallower settings and they occur in euryhaline environments; and (4) *Orthobairdia* are predominantly distributed in distal platform environments.

The species composition with the presence of *Orthobairdia* in the *Paratirolites* Limestone and *Microcheilinella*, small Cavellinidae, Kirkbyidae and *Basslerella* in the Aras Member confirms the already published environmental interpretation, which suggested a deep shelf setting throughout the investigated part of the section with no large-scale bathymetric changes (Leda *et al.* 2014; Gliwa *et al.* 2020a). Relatively high occurrences of cavellinids in the lower half of the Aras Member may indicate a more proximal setting, which is not supported by the

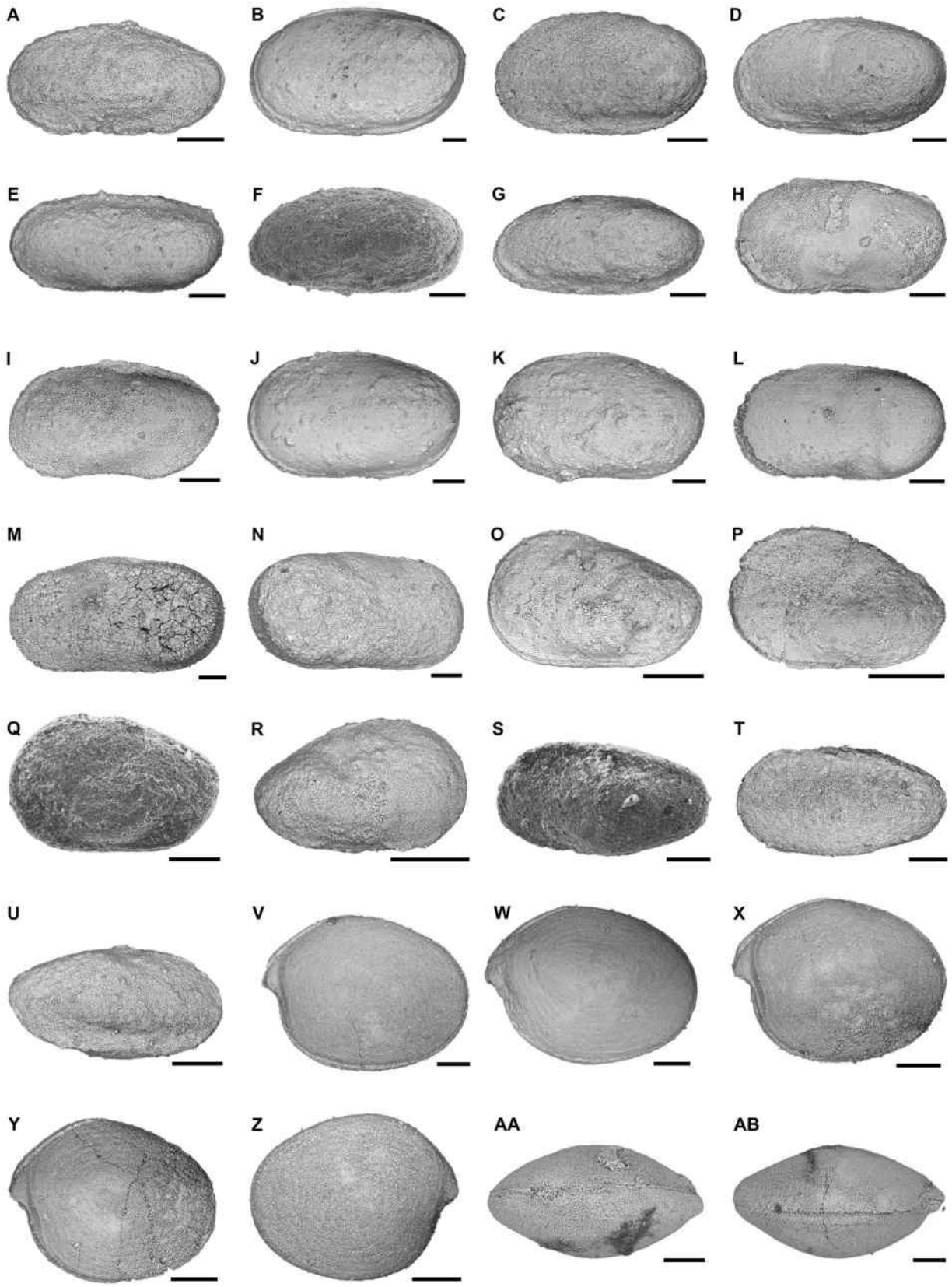


FIG. 24. SEM micrographs of ostracods from the Aras Valley section, north-west Iran. A, *Cavellina* sp. 1, AV028X-13, left lateral view. B–D, *Cavellina* sp. 2: B, AV265SH-65, left lateral view; C, AV088-40, left lateral view; D, AV075SH-29, left lateral view. E–G, *Cavellina* sp. 3: E, AV116Y-20, left lateral view; F, AV075SH-16, left lateral view; G, AV125SH-101, left lateral view. H–I, *Cavellina* sp. 4: H, AV260-42, left lateral view; I, AV260-54, left lateral view. J–K, *Cavellina* sp. 5: J, AV265SH-69, left lateral view; K, AV265SH-58, left lateral view. L–N, *Sulcella* sp. 1: L, AV260-33, left lateral view; M, AV310-39, left lateral view; N, AV288SH-159, right lateral view. O–R, *Callicythere* sp. 1: O, AV138FO-33, left lateral view; P, AV088X-28, left lateral view; Q, AV075SH-02, left lateral view; R, AV075SH-50, right lateral view. S–U, *Callicythere* sp. 2: S, AV103SH-06, left lateral view; T, AV125SH-41, left lateral view; U, AV116SH-75, right lateral view. V–AB, *Hungaroleberis striatus* Forel, sp. nov.: V, holotype ECO124, left lateral view; W, paratype ECO125, left lateral view; X, AVn330-59, left lateral view; Y, AVn330-17, left lateral view; Z, AVn330-52, right lateral view; AA, AVn330-28, dorsal view; AB, holotype ECO124, ventral view. Scale bars represent 100 μm .

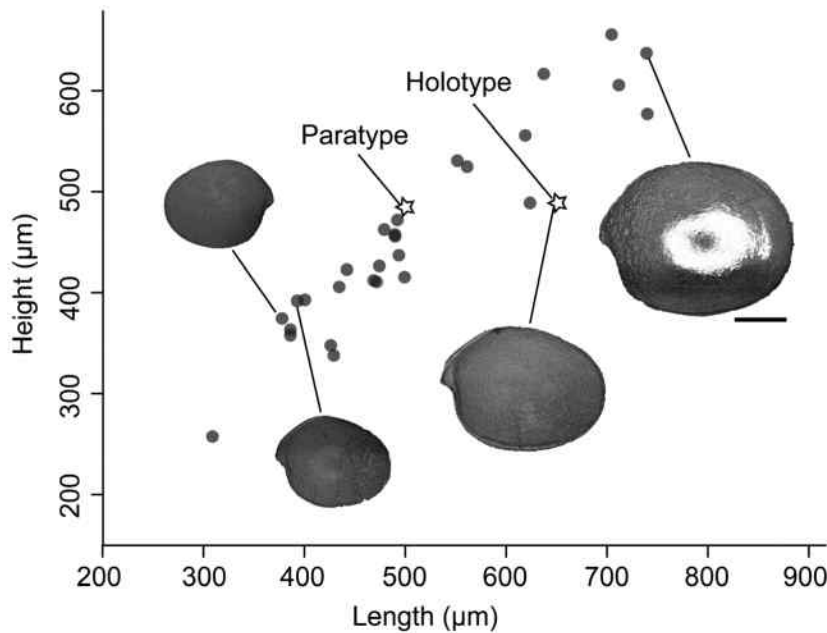


FIG. 25. Length/height scatter plot of *Hungaroleberis striatus* Forel, sp. nov. from the Aras Valley section. Displayed specimens from left to right: AVn330-52, AVn330-17, ECO124, AVn330-09. Scale bar represents 200 μm .

microfacies analysis of this section interval (Gliwa *et al.* 2020a). Furthermore, the high number of bairdiid species (Fig. 27) indicates that the investigated part of the section was formed under normal marine conditions with normal salinity.

Low-diversity Paratirolites Limestone and EPME/extinction horizon. The very low diversity in the upper *Paratirolites* Limestone terminates in a monospecific assemblage with *Fabalicypriis obunca* in the uppermost sample horizon (–0.01 m). In the marine, littoral habitat, the diversity of ostracod assemblages is mostly constrained by water energy, sediment substrate type, salinity, nutrient availability, concentration of dissolved oxygen, temperature and their fluctuations (Benson *et al.* 1983; Dingle & Girardeau 1993; Hinz-Schallreuter & Schallreuter 1999; Frenzel & Boomer 2005). The samples from the Aras Valley section were deposited in an outer shelf environment below the storm wave base, in a low-energy environment (Leda *et al.* 2014; Gliwa *et al.* 2020a). The sediment substrate throughout the section consisted of fine-grained

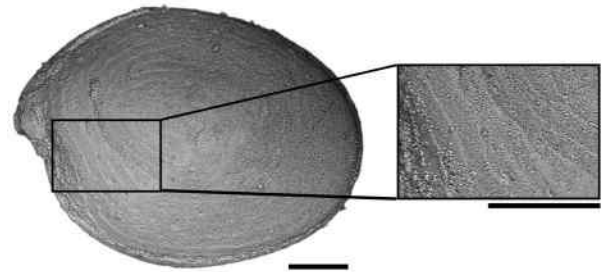


FIG. 26. Specimen of *Hungaroleberis striatus* Gliwa, sp. nov. (paratype, ECO125) with magnified striated surface structure. Scale bars represent 100 μm .

carbonate mud with a varying clay content (Gliwa *et al.* 2020a). A significant change of diversity and composition between the assemblages, caused by variable substrate type or water energy, is, therefore, not expected in the studied section interval.

Given that most of the marine ostracod species are stenohaline, salinity changes have a major influence on

TABLE 1. Ostracod assemblages of the *Paratirolites* Limestone of the Aras Valley (north-west Iran) with all identified species.

Class OSTRACODA Latreille, 1806	Superfamily CYPRIDOIDEA Baird, 1845
Subclass PODOCOPA Müller, 1894	Family PARACYPRIDIDAE Sars, 1923
Order PODOCOPIDA Sars, 1866	<i>Paracypris</i> sp. 1
Suborder PODOCOPINA Gründel, 1967	Order PALAEOCOPIDA Henningsmoen, 1953
Superfamily BAIRDIOIDEA Sars, 1887	Suborder BEYRICHICOPINA Scott, 1961
Family BAIRDIIDAE Sars, 1887	Superfamily HOLLINOIDEA Swartz, 1936
<i>Fabalicypris obunca</i> Belousova, 1965	Family HOLLINELLIDAE Bless & Jordan, 1971
<i>Fabalicypris blumenstengeli</i> Crasquin, 2008	<i>Hollinella</i> sp. 1
<i>Orthobairdia capuliformis</i> Gliwa, sp. nov.	Subclass MYODOCOPA Sars, 1866
<i>Araxobairdia formosa</i> Gliwa, gen. et sp. nov.	Order MYODOCOPIDA Sars, 1866
<i>Bairdia</i> sp. 1	Suborder MYODOCOPINA Sars, 1866
Family indet.	Superfamily CYLINDROLEBERIDOIDEA Müller, 1906
<i>Eumiraculum mettei</i> Gliwa, sp. nov.	Family CYLINDROLEBERIDIDAE Müller, 1906
	<i>Hungaroleberis striatus</i> Forel, sp. nov.

TABLE 2. Ostracod assemblages of the Aras Member of the Aras Valley (north-west Iran) with all identified species.

Subclass PODOCOPA Müller, 1894	Superfamily SIGILLIOIDEA Mandelstam, 1960
Order PODOCOPIDA Sars, 1866	Family MICROCHEILINELLIDAE Gramm, 1975
Suborder PODOCOPINA Gründel, 1967	<i>Microcheilinella</i> cf. <i>perexilis</i> Shi, 1987
Superfamily BAIRDIOIDEA Sars, 1887	<i>Microcheilinella</i> sp. 1
Family BAIRDIIDAE Sars, 1887	<i>Microcheilinella</i> sp.
<i>Bairdia hassi</i> Sohn, 1960	Suborder CYPRIDOCOPINA Jones, 1901
<i>Bairdia</i> cf. <i>piscariformis</i> Chen, 1958	Superfamily CYPRIDOIDEA Baird, 1845
<i>Bairdia</i> sp. 2	Family PARACYPRIDIDAE Sars, 1923
<i>Bairdia</i> sp. 3	<i>Paracypris gaetanii</i> Crasquin-Soleau, 2006
<i>Bairdia</i> sp. 4	<i>Paracypris</i> sp. 2
<i>Bairdiacypris kathleenae</i> Gliwa, sp. nov.	Suborder METACOPINA Sylvester-Bradley, 1961
<i>Bairdiacypris ottomanensis</i> Crasquin-Soleau, 2004	Superfamily HEALDIOIDEA Harlton, 1933
<i>Bairdiacypris zaliensis</i> Mette, 2010	Family HEALDIIDAE Harlton, 1933
<i>Bairdiacypris</i> sp. 1	<i>Hungarella</i> sp. 1
<i>Bairdiacypris</i> sp. 2	Order PALAEOCOPIDA Henningsmoen, 1953
<i>Bairdiacypris</i> sp. 3	Suborder KIRKBYOCOPINA Gründel, 1969
<i>Bairdiacypris</i> sp. 4	Superfamily KIRKBYOIDEA Ulrich & Bassler, 1906
<i>Fabalicypris veronicae</i> Gliwa, sp. nov.	Family KIRKBYIDAE Ulrich & Bassler, 1906
<i>Fabalicypris</i> cf. <i>minuta</i> Cooper, 1946	<i>Iranokirkbya brandneri</i> Kozur & Mette, 2006
<i>Fabalicypris</i> sp. 1	<i>Carinaknightina hofmanni</i> Gliwa, sp. nov.
<i>Fabalicypris</i> sp. 2	<i>Reviya</i> sp. 1
<i>Fabalicypris</i> sp. 3	Suborder, superfamily, family indet.
<i>Kempfina</i> sp. 1	<i>Buregia?</i> sp. 1
<i>Kempfina</i> sp. 2	Order PLATYCOPIDA Sars, 1866
<i>Kempfina qinglaii</i> (Crasquin), 2008	Suborder PLATYCOPINA Sars, 1866
<i>Praezabythocypris pulchra</i> Kozur, 1985	Superfamily CAVELLINOIDEA Egorov, 1950
<i>Praezabythocypris</i> cf. <i>pulchra</i> sensu Forel, 2014	Family CAVELLINIDAE Egorov, 1950
Family indet.	<i>Cavellina fosteri</i> Gliwa, sp. nov.
<i>Liuzhinia?</i> sp. 1	<i>Cavellina araxensis</i> Gliwa, sp. nov.
<i>Liuzhinia julfensis</i> Gliwa, sp. nov.	<i>Cavellina</i> sp. 1
<i>Liuzhinia antalyaensis</i> Crasquin-Soleau, 2004	<i>Cavellina</i> sp. 2
Superfamily CYTHEROIDEA Baird, 1850	<i>Cavellina</i> sp. 3
Family BYTHOCYTHERIDAE Sars, 1928	<i>Cavellina</i> sp. 4
<i>Callicythere</i> sp. 1	<i>Sulcella</i> sp. 1
<i>Callicythere</i> sp. 2	
Family CYTHERIDEIDAE Sars, 1925	
<i>Basslerella</i> sp. 1	

TABLE 3. Ostracod assemblages of the *Claraia* Beds of the Aras Valley (north-west Iran) with all identified species.

Subclass PODOCOPA Müller, 1894	Order PALAEOCOPIA Henningsmoen, 1953
Order PODOCOPIDA Sars, 1866	Suborder KLOEDENELLOCOPINA Scott, 1961
Suborder PODOCOPINA Gründel, 1967	Superfamily KLOEDENELLOIDEA Ulrich & Bassler, 1908
Superfamily BAIRDIOIDEA Sars, 1887	Family INDIVISIIDAE Egorov, 1954
Family BAIRDIIDAE Sars, 1887	<i>Indivisia</i> sp. 1
<i>Bairdiacypris kathleenae</i> Gliwa, sp. nov.	<i>Indivisia</i> sp. 2
<i>Bairdiacypris ottomanensis</i> Crasquin-Soleau, 2004	Superfamily PARAPARCHITOIDEA Scott, 1959
<i>Bairdiacypris</i> cf. <i>longirobusta</i> Chen, 1958	Family PARAPARCHITIDAE Scott, 1959
<i>Bairdiacypris</i> sp. 1	<i>Langaia</i> sp. 1
<i>Bairdiacypris</i> sp. 2	Suborder, superfamily, family indet.
<i>Bairdiacypris</i> sp. 3	<i>Buregia?</i> sp. 1
<i>Bairdiacypris</i> sp. 4	Suborder CYPRIDOCOPINA Jones, 1901
<i>Praezabythocypris pulchra</i> Kozur, 1985	Superfamily CYPRIDOIDEA Baird, 1845
<i>Praezabythocypris</i> cf. <i>pulchra</i> Kozur, 1985	Family PARACYPRIDIDAE Sars, 1923
<i>Bairdia?</i> <i>kemerensis</i> Crasquin-Soleau, 2004	<i>Paracypris gaetanii</i> Crasquin-Soleau, 2006
<i>Bairdia</i> cf. <i>piscariformis</i> Chen, 1958	Order PLATYCOPIA Sars, 1866
<i>Bairdia</i> sp. 5	Suborder PLATYCOPIA Sars, 1866
<i>Fabalitypris</i> sp. 1	Superfamily CAVELLINOIDEA Egorov, 1950
<i>Fabalitypris</i> sp. 2	Family CAVELLINIDAE Egorov, 1950
<i>Fabalitypris</i> sp. 3	<i>Cavellina</i> sp. 2
Family indet.	<i>Cavellina</i> sp. 4
<i>Liuzhinia julfensis</i> Gliwa, sp. nov.	<i>Cavellina</i> sp. 5
<i>Liuzhinia antalyaensis</i> Crasquin-Soleau, 2004	
<i>Liuzhinia</i> sp. 2	

their distribution (Mesquita-Joanes *et al.* 2012). Faunal changes linked to salinity changes are mainly recognized in marginal marine, coastal environments, where terrestrial freshwater input lowers salinity and constrains the distribution of marine ostracod species (Frenzel & Boomer 2005). A major change in salinity, caused by freshwater input, is not suspected for the Aras Valley section because of the lack of indications of prominent terrigenous input, implying a large distance to the coastline. Furthermore, high numbers of specimens of the Bairdiidae, which are usually found within a normal marine salinity range (Kornicker 1961; Crasquin-Soleau *et al.* 1999), were present throughout the analysed interval of the Aras Valley section.

Although some Recent ostracod species are known to tolerate low oxygen levels, or even prefer it; they are able to survive within hypoxic conditions for a short time (Jahn *et al.* 1996; Modig & Ólafsson 1998; Rossi *et al.* 2002; Corbari *et al.* 2004). However, ostracods in general are very sensitive to oxygen level changes and depletion (Buhl-Mortensen *et al.* 2009). Low oxygen conditions in the marine habitat usually lead to a decreased diversity of ostracods (Modig & Ólafsson 1998; Buhl-Mortensen *et al.* 2009). The low-diversity ostracod assemblage of the *Paratiro-lites* limestone in the Aras Valley section may, therefore, be caused by a decrease in dissolved oxygen, leading to the local disappearance of the species. Uranium isotopes from the nearby Zal section indicate an onset of

anoxic conditions at the EPME (Zhang *et al.* 2018). However, in the present study as well as in other north-west Iranian sections, the low diversity of the *Paratiro-lites* Limestone is also paralleled by the occurrence of other oxygen-dependent organisms such as ammonoids, sponges, gastropods, bivalves and echinoderms (Leda *et al.* 2014; Gliwa *et al.* 2020a). Evidence for a bioturbated sea floor up to the uppermost bed of the *Paratiro-lites* Limestone (Gliwa *et al.* 2020a) indicates normal marine oxygen concentrations of the bottom waters.

Temperature was identified as a major influence on the diversity and population size of marine assemblages (Heip 1976; Cronin 1991; Cronin *et al.* 1995), although studies of fossil and extant ostracods indicate that few species appear to have an extreme thermal tolerance window (e.g. Kulköylüoğlu *et al.* 2003). Unstable environmental conditions, such as sealevel fluctuation, as well as high sealevels, which are accompanied by temperature change in the habitat, lead to lower ostracod diversity (Slipper 2005; Crasquin *et al.* 2010). Regarding for example the fossil record of the Early Toarcian warming, it was suggested that a decrease in ostracod diversity and the extinction of many species, can be connected to a rapid temperature increase (Gómez & Arias 2010). The dramatic temperature increase of c. 7–10°C at the EPME in north-west Iran is assumed to have started directly at the extinction horizon (Schobben *et al.* 2014). This coincides with the disappearance of *Fabalitypris obunca* and the

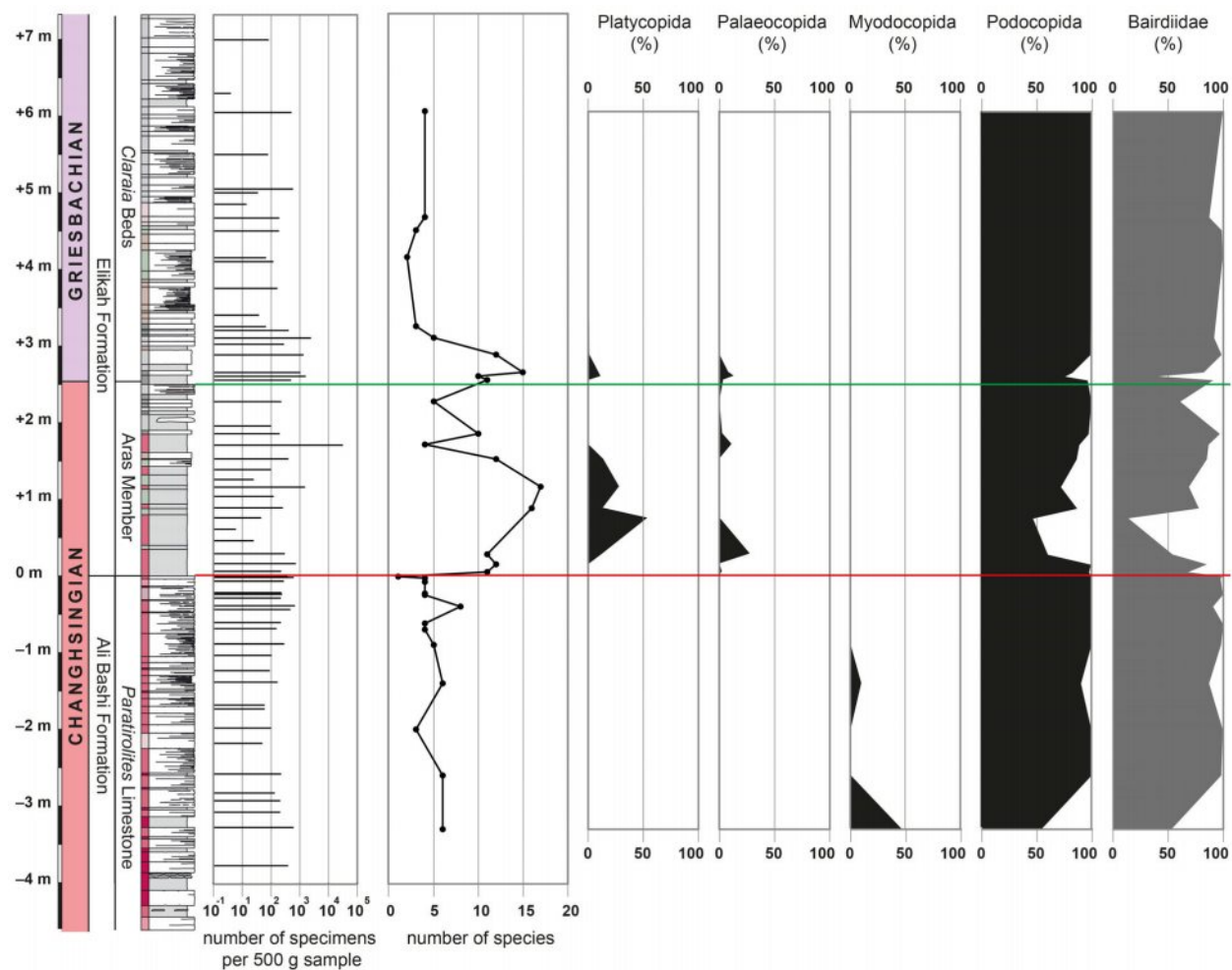


FIG. 27. Diversity and taxonomic patterns of the Aras Valley section. From left to right: Quantity of specimens per 500 g sample material; species richness per sample horizon (only samples with >40 identified specimens were taken into account); percentage of specimens per order (black area) and percentage of identified Bairdiidae specimens (grey area) in the total amount of identified specimens (only samples with >40 identified specimens were taken into account). The lower (red) and upper (green) horizontal lines mark the extinction event and the Permian–Triassic boundary. Colour online.

complete faunal turnover at the transition to the Aras Member. Consequently, a linkage between the rapid temperature change and the impoverishment of the ostracod fauna is possible. Rapid warming may have exceeded the temperature tolerance limit of *F. obunca* and led to the extinction of the species and to the replacement of the community in the Aras Valley section.

High post-extinction diversity. Compared with the *Paratirolites* Limestone, the post-extinction assemblages from the Aras Member represent a more diverse benthic ostracod community even at a higher taxonomic level (Fig. 27). Relatively diverse ostracod assemblages in the aftermath of the EPME have also been recorded from

very proximal siliciclastic environments (Crasquin *et al.* 2017) or in association with microbial build-ups (Forel *et al.* 2009, 2013, 2015; Forel 2012, 2014). This led to the hypothesis of a microbial refuge, which protected ostracods from an assumed oxygen-poor environment. The high abundance and diversity of ostracods in the Aras Valley section is not associated with microbialites, which indicates that these assemblages were probably not stressed by large-scale environmental changes, such as changes in dissolved oxygen concentrations. This is also suggested by the occurrence of Bairdiidae, which were found throughout the investigated interval. Bairdiidae are usually found in marine environments that are well-oxygenated (Kornicker 1961; Maddocks 1969; Melnyk &

Maddocks 1988) and indicate normal marine salinity (Kornicker 1961; Crasquin-Soleau *et al.* 1999). Their presence in the entire investigated section interval and their predominance in the assemblages, except from the lower third of the Aras Member (Fig. 27) indicate that the post-extinction assemblages were also not suffering low oxygen concentrations or strong salinity changes.

The temperature reconstruction for the Permian–Triassic transition in South China and north-west Iran (Joachimski *et al.* 2012; Sun *et al.* 2012; Schobben *et al.* 2014) shows that the post-extinction interval is characterized by high-temperature seawater (*c.* 38°C). In general, the thermal tolerance of marine ostracods is still poorly characterized. However, a summary of marine Eocene taxa (e.g. Hazel & Holden 1971) shows that many of them are eurythermal. Ostracods have, in contrast to many other marine organisms, such as cephalopods, foraminifers or echinoderms, a very broad temperature tolerance (Ganning 1971) and some species have a comparatively high thermal limit, which was demonstrated for freshwater species (Wickstrom & Castenholz 1973, 1985; Kulköylüoğlu *et al.* 2003; Kulköylüoğlu 2004; Vandekerckhove *et al.* 2013). For example, specimens of *Thermopsis thermophila* were even found in hot springs at water temperatures above 50°C (Kulköylüoğlu *et al.* 2003). This could indicate that some species were able to tolerate the presumably hot post-extinction climate.

CONCLUSIONS

In the Aras Valley section (north-west Iran), which spans the EPME and the PTB, 59 sampled horizons yielded ostracods.: We report here on the occurrence of 62 species, of which ten species and one genus are new: *Fabaliocypris veronicae* Gliwa, sp. nov., *Orthobairdia capuliformis* Gliwa, sp. nov., *Araxobairdia formosa* Gliwa, gen. et sp. nov., *Bairdiocypris kathleenae* Gliwa, sp. nov., *Eumiraculum mettei* Gliwa, sp. nov., *Liuzhinia julfensis* Gliwa, sp. nov., *Carinaknightina hofmanni* Gliwa, sp. nov., *Cavellina fosteri* Gliwa, sp. nov., *Cavellina hairapetiani* Gliwa, sp. nov. and *Hungaroleberis striatus* Forel, sp. nov.

The species compositions of all samples represent a typical tropical marine environment. The occurrences of taxa, which are usually found in distal platform environments (*Microcheilinella*, *Orthobairdia*, *Basslerella* and *Kirkbyidae*) confirm a deep shelf setting without large-scale bathymetric changes, as already suggested from the microfacies analysis. Furthermore, a high number of occurrences of the Bairdiidae, which are present throughout the entire succession, indicate open marine conditions with normal marine salinity and oxygen concentrations.

The pre-extinction ostracod assemblage of the *Paratiro-lites* Limestone is dominated by *Fabaliocypris obunca*,

which forms a monospecific assemblage in the uppermost sample. The low diversity of this assemblage may be caused by depleted oxygenation of the habitat, although sedimentological and palaeontological investigations of the studied section, as well as neighbouring sections, suggest an oxygenated environment. The subsequent total faunal turnover at the EPME and the transition from the *Paratiro-lites* Limestone to the Aras Member ('Boundary Clay') coincides with the massive temperature increase, which was determined for north-west Iran. The post-extinction assemblages are dominated by *Bairdiocypris ottomanensis* and show a relatively high diversity in the immediate aftermath of the EPME. Compared with other diverse ostracod assemblages from the Palaeotethyan realm, the ostracods of the Aras Valley section are not associated with microbialites.

Acknowledgements. We are indebted to the Aras Free Zone Office (Julfa) for logistical support for the field sessions. We thank Kathleen Schindler (Berlin) for processing the ostracod samples. Many thanks to William J. Foster (Dublin) for discussions and his helpful comments on the manuscript. Furthermore we are indebted to Avraham Honigstein (Jerusalem), Frank Scholze (Darmstadt), Gengo Tanaka (Kanazawa) and an anonymous reviewer for reviews of an earlier version of the manuscript. For financial support of the project, we acknowledge the Deutsche Forschungsgemeinschaft (DFG project Ko1829/18-1) and the TERSANE research group (FOR 2332).

DATA ARCHIVING STATEMENT

This published work and the nomenclatural acts it contains, have been registered in ZooBank: <http://zoobank.org/References/E6A6F765-45C0-43A9-B3BD-1E3446BAD2B0>
Data for this study are available in the *Dryad Digital Repository*: <https://doi.org/10.5061/dryad.dncjsxkwc>

Editor. Yue Wang

REFERENCES

- ARAKELYAN, R. A., GRUNT, T. A. and SHEVYREV, A. A. 1965. Kratkiy stratigraficheskiy ocherk. 20–25. In RYZHENCEV, V.E. and SARYTCHEVA, T.G. (eds). *Rasvitie i smena morskikh organizmov na rubezhe Paleozoya i Mezozoya*. Trudy Paleontologicheskogo Instituta Akademii Nauk SSSR, **108**. [in Russian]
- BAIRD, W. 1845. Arrangement of the British Entomostraca, with a list of species, particularly noticing those which have as yet been discovered within the bounds of the Club. *History of the Berwickshire Naturalists' Club*, **2**, 145–158.
- 1850. *The natural history of the British Entomostraca*. Ray Society, London, 364 pp.
- BELOUSOVA, Z. 1965. Evolution and succession of organisms at Paleozoic-Mesozoic boundary. *Trudy Paleontologicheskogo Instituta Akademii Nauk SSSR*, **108**, 245–265.

- BENSON, R. H., DELGROSSO, R. M. and STEINECK, P. L. 1983. Ostracode distribution and biofacies, Newfoundland continental slope and rise. *Micropaleontology*, **29**, 430–453.
- BIJMA, J., PÖRTNER, H.-O., YESSON, C. and ROGERS, A. D. 2013. Climate change and the oceans: what does the future hold? *Marine Pollution Bulletin*, **74**, 495–505.
- BLESS, M. J. M. and JORDAN, H. 1971. Classification of Palaeocopid ostracodes belonging to the families Ctenoloculiniidae, Hollinidae and Hollinellidae. *Bulletin Centre de Recherche Pau-SNPA*, **5**, 869–890.
- BOND, D. P. and GRASBY, S. E. 2017. On the causes of mass extinctions. *Palaeogeography, Palaeoclimatology, Palaeoecology*, **478**, 3–29.
- BOOMER, I., HORNE, D. J. and SLIPPER, I. J. 2003. The use of ostracods in palaeoenvironmental studies, or what can you do with an ostracod shell? *The Paleontological Society Papers*, **9**, 153–180.
- BRADFIELD, H. H. 1935. Pennsylvanian Ostracoda of the Ardmore Basin, Oklahoma. *Bulletins of American Paleontology*, **22**, 1–173.
- BRENNECKA, G. A., HERRMANN, A. D., ALGEO, T. J. and ANBAR, A. D. 2011. Rapid expansion of oceanic anoxia immediately before the end-Permian mass extinction. *Proceedings of the National Academy of Sciences*, **108**, 17631–17634.
- BROUWERS, E. M. 1988. Sediment transport detected from the analysis of ostracod population structure: an example from the Alaskan continental shelf. 231–244. In DE DECKKER, P., COLIN, J.-P. and PEYPOUQUET, J.-P. (eds). *Ostracoda in the earth sciences*. Elsevier.
- BUHL-MORTENSEN, L., OUG, E. and AURE, J. 2009. The response of hyperbenthos and infauna to hypoxia in fjords along the Skagerrak: estimating loss of biodiversity due to eutrophication. 79–96. In MOKSNESS, E., DAHL, E. and STØTTRUP, J. (eds). *Integrated coastal zone management*. Wiley-Blackwell.
- BURGESS, S. D. and BOWRING, S. A. 2015. High-precision geochronology confirms voluminous magmatism before, during, and after Earth's most severe extinction. *Science Advances*, **1**, e1500470.
- CHEN, T. 1958. Permian ostracods from the Chihsia limestone of Lungtan, Nanking. *Acta Palaeontologica Sinica*, **6**, 215–257.
- CHEN, D. Q. and SHI, C. G. 1982. Latest Permian Ostracoda from Nantong, Jiangsu and from Mianyang, Hubei. *Bulletin of Nanjing Institute of Geology & Palaeontology, Academia Sinica*, **4**, 105–152.
- CLARKSON, M., WOOD, R., POULTON, S., RICHOSZ, S., NEWTON, R., KASEMANN, S., BOWYER, F. and KRISTYN, L. 2016. Dynamic anoxic ferruginous conditions during the end-Permian mass extinction and recovery. *Nature Communications*, **7**, 12236.
- COOPER, C. L. 1946. Pennsylvanian ostracodes of Illinois. *Bulletin of the Geological Survey of Illinois*, **70**, 1–177.
- CORBARI, L., CARBONEL, P. and MASSABUAU, J.-C. 2004. How a low tissue O₂ strategy could be conserved in early crustaceans: the example of the podocopid ostracods. *Journal of Experimental Biology*, **207**, 4415–4425.
- CORYELL, H. N. 1928. Some new Pennsylvanian ostracoda. *Journal of Paleontology*, **2**, 87–94.
- COSTANZO, G. V. and KAESLER, R. L. 1987. Changes in Permian marine ostracode faunas during regression, Florena shale, Northeastern Kansas. *Journal of Paleontology*, **61**, 1204–1215.
- CRASQUIN, S. and FOREL, M.-B. 2014. Ostracods (Crustacea) through Permian–Triassic events. *Earth-Science Reviews*, **137**, 52–64.
- PERRI, M. C., NICORA, A. and DE WEVER, P. 2008. Ostracods across the Permian–Triassic boundary in Western Tethys: the Bulla parastratotype (Southern Alps, Italy). *Rivista Italiana di Paleontologia e Stratigrafia*, **114**, 233–262.
- FOREL, M.-B., QINGLAI, F., AIHUA, Y., BAUDIN, F. and COLLIN, P.-Y. 2010. Ostracods (Crustacea) through the Permian–Triassic boundary in South China: the Meishan stratotype (Zhejiang Province). *Journal of Systematic Palaeontology*, **8**, 331–370.
- — YUAN, A., NESTELL, G. and NESTELL, M. 2017. Species of Hollinella (Palaeocopida: Ostracoda: Crustacea) as stratigraphical indices of the Late Permian–Early Triassic post-extinction interval. *Journal of Systematic Palaeontology*, **16**, 213–224.
- CRASQUIN-SOLEAU, S. and BAUD, A. 1998. New Permian ostracods from Greece (Hydra Island). *Journal of Micropalaeontology*, **17**, 131–152.
- and KERSHAW, S. 2005. Ostracod fauna from the Permian–Triassic boundary interval of South China (Huaying Mountains, eastern Sichuan Province): palaeoenvironmental significance. *Palaeogeography, Palaeoclimatology, Palaeoecology*, **217**, 131–141.
- BROUTIN, J., ROGER, J., PLATEL, J.-P., AL HASHMI, H., ANGIOLINI, L., BAUD, A., BUCHER, H. and MARCOUX, J. 1999. First Permian ostracode fauna from the Arabian Plate (Khuff Formation, Sultanate of Oman). *Micropaleontology*, **45**, 163–182.
- MARCOUX, J., ANGIOLINI, L. and NICORA, A. 2004a. Palaeocopida (Ostracoda) across the Permian–Triassic events: new data from southwestern Taurus (Turkey). *Journal of Micropalaeontology*, **23**, 67–76.
- — RICHOSZ, S., NICORA, A., BAUD, A. and BERTHO, Y. 2004b. A new ostracode fauna from the Permian–Triassic boundary in Turkey (Taurus, Antalya Nappes). *Micropaleontology*, **50**, 281–295.
- GALFETTI, T., BUCHER, H. and BRAYARD, A. 2006a. Palaeoecological changes after the end-Permian mass extinction: Early Triassic ostracods from northwestern Guangxi Province, South China. *Rivista Italiana di Paleontologia e Stratigrafia*, **112**, 55–75.
- VASLET, D. and LE NINDRE, Y. 2006b. Ostracods of the Permian–Triassic Khuff Formation, Saudi Arabia: palaeoecology and palaeobiogeography. *GeoArabia, Gulf Petrolink, Bahrain*, **11**, 55–76.
- CRONIN, T. M. 1991. Pliocene shallow water paleoceanography of the North Atlantic Ocean based on marine ostracodes. *Quaternary Science Reviews*, **10**, 175–188.
- HOLTZ JR, T., STEIN, R., SPIELHAGEN, R., FÜTTERER, D. and WOLLENBURG, J. 1995. Late Quaternary

- paleoceanography of the Eurasian Basin, Arctic Ocean. *Paleoceanography*, **10**, 259–281.
- DINGLE, R. and GIRAudeau, J. 1993. Benthic Ostracoda in the Benguela System (SE Atlantic): a multivariate analysis. *Marine Micropaleontology*, **22**, 71–92.
- EGOROV, V. 1950. *Frasnian ostracods from Russian platform. I. Kloedenellitidae*. VNIGRI (All Russia Petroleum Research Exploration Institut), 175 pp. [in Russian]
- 1954. *Indivisiinae. A new family of Kloedenellidae from the Frasnian strata of Russian platform*. VNIGRI (All Russia Petroleum Research Exploration Institut), **1**, 5–21. [in Russian]
- ERWIN, D. H. 1994. The Permo-Triassic extinction. *Nature*, **367**, 231–236.
- FOREL, M.-B. 2012. Ostracods (Crustacea) associated with microbialites across the Permian–Triassic boundary in Dajiang (Guizhou Province, south China). *European Journal of Taxonomy*, **19**, 1–34.
- 2014. Heterochronic growth of ostracods (Crustacea) from microbial deposits in the aftermath of the end-Permian extinction. *Journal of Systematic Palaeontology*, **13**, 315–349.
- and CRASQUIN, S. 2011. Lower Triassic ostracods (Crustacea) from the Meishan section, Permian–Triassic boundary GSSP (Zhejiang Province, South China). *Journal of Systematic Palaeontology*, **9**, 455–466.
- — KERSHAW, S., FENG, Q. and COLLIN, P.-Y. 2009. Ostracods (Crustacea) and water oxygenation in the earliest Triassic of South China: implications for oceanic events at the end-Permian mass extinction. *Australian Journal of Earth Sciences*, **56**, 815–823.
- — BRÜHWILER, T., GOUEMAND, N., BUCHER, H., BAUD, A. and RANDON, C. 2011. Ostracod recovery after Permian–Triassic boundary mass-extinction: the south Tibet record. *Palaeogeography, Palaeoclimatology, Palaeoecology*, **308**, 160–170.
- — HIPS, K., KERSHAW, S., COLLIN, P.-Y. and HAAS, J. 2013. Biodiversity evolution through the Permian–Triassic boundary event: ostracods from the Bükk Mountains, Hungary. *Acta Palaeontologica Polonica*, **58**, 195–219.
- — CHITNARIN, A., ANGIOLINI, L. and GAETANI, M. 2015. Precocious sexual dimorphism and the Lilliput effect in Neo-Tethyan Ostracoda (Crustacea) through the Permian–Triassic boundary. *Palaeontology*, **58**, 409–454.
- THUY, B. and WISSHAK, M. 2019. Digging into the ancestral stocks of Jurassic lineages: ostracods (Crustacea) from Carnian (Late Triassic) sponge mounds from the Maantang Formation (South China). *BSGF Earth Sciences Bulletin*, **190** (9), 1–29.
- FRENZEL, P. and BOOMER, I. 2005. The use of ostracods from marginal marine, brackish waters as bioindicators of modern and Quaternary environmental change. *Palaeogeography, Palaeoclimatology, Palaeoecology*, **225**, 68–92.
- GANNING, B. 1971. On the ecology of *Heterocypris salinus*, *H. incongruens* and *Cypridopsis aculeata* (Crustacea: Ostracoda) from Baltic brackish-water rockpools. *Marine Biology*, **8**, 271–279.
- GHADERI, A. 2014. Stratigraphy and paleoecology of the Upper Permian to Permian–Triassic boundary in the northwest of Iran based on biostratigraphic data of conodonts and brachiopods. PhD thesis, Ferdowsi University of Mashhad, 488 pp.
- LEDA, L., SCHOBEN, M., KORN, D. and ASHOURI, A. R. 2014a. High-resolution stratigraphy of the Changhsingian (Late Permian) successions of NW Iran and the Transcaucasus based on lithological features, conodonts and ammonoids. *Fossil Record*, **17**, 41–57.
- GARBELLI, C., ANGIOLINI, L., ASHOURI, A. R., KORN, D., RETTORI, R. and GHARAIE, M. H. M. 2014b. Faunal change near the end-Permian extinction: the brachiopods of the Ali Bashi Mountains, NW Iran. *Rivista Italiana di Paleontologia e Stratigrafia*, **120**, 27–59.
- GLIWA, J., GHADERI, A., LEDA, L., SCHOBEN, M., TOMÁS, S., FOSTER, W. J., FOREL, M.-B., GHANIZADEH TABRIZI, N., GRASBY, S. E., STRUCK, U., ASHOURI, A. R. and KORN, D. 2020a. Aras Valley (Northwest Iran): high-resolution stratigraphy of a continuous central Tethyan Permian–Triassic boundary section. *Fossil Record*, **23**, 33–69.
- FOREL, M.-B., CRASQUIN, S., GHADERI, A. and KORN, D. 2020b. Data from: Ostracods from the end-Permian mass extinction in the Aras Valley section (north-west Iran). *Dryad Digital Repository*. <https://doi.org/10.5061/dryad.dncjsxkwc>
- GÓMEZ, J. and ARIAS, C. 2010. Rapid warming and ostracods mass extinction at the Lower Toarcian (Jurassic) of central Spain. *Marine Micropaleontology*, **74**, 119–135.
- GRAMM, M. N. 1975. Ostracods of the genus *Microcheilina* in the Middle Triassic of the southern Primorye. *Paleontologicheskij Zhurnal*, **3**, 83–88.
- GRASBY, S., BEAUCHAMP, B., EMBRY, A. and SANEI, H. 2013. Recurrent Early Triassic ocean anoxia. *Geology*, **41**, 175–178.
- GRÜNDEL, J. 1967. Zur Grossgliederung der Ordnung Podocopida G. W. Müller, 1894. *Neues Jahrbuch für Geologie & Paläontologie, Monatshefte*, **6**, 321–332.
- 1969. Neue taxonomische Einheiten der Unterklasse Ostracoda (Crustacea). *Neues Jahrbuch für Geologie und Paläontologie, Monatshefte*, **6**, 353–361.
- HAO, W. 1996. Ostracods from the Upper Permian and Lower Triassic of the Zhenfeng Section, South China. *Journal of Geosciences, Osaka City University*, **39**, 19–27.
- HARLTON, B. H. 1927. Some Pennsylvanian Ostracoda of the Glenn and Hoxbar Formations of southern Oklahoma and of the upper part of the Cisco Formation of northern Texas. *Journal of Paleontology*, **1**, 203–212.
- 1933. Micropaleontology of the Pennsylvanian Johns Valley Shale of Ouachita Mountains, Oklahoma and its relationships to the Mississippian Caney Shale. *Journal of Paleontology*, **7**, 3–29.
- HAZEL, J. E. and HOLDEN, J. C. 1971. Ostracoda of Late Eocene age from Eua, Tonga. *Geological Survey Professional Paper*, **640-D**, D1–D11.
- HEIP, C. 1976. The life-cycle of *Cyprideis torosa* (Crustacea, Ostracoda). *Oecologia*, **24**, 229–245.
- HENNINGSMOEN, G. 1953. Classification of Paleozoic straight-hinged ostracods. *Norsk Geologisk Tidsskrift*, **31**, 185–290.
- HINOJOSA, J. L., BROWN, S. T., CHEN, J., DEPAOLO, D. J., PAYTAN, A., SHEN, S.-Z. and PAYNE, J. L. 2012.

- Evidence for end-Permian ocean acidification from calcium isotopes in biogenic apatite. *Geology*, **40**, 743–746.
- HINZ-SCHALLREUTER, I. and SCHALLREUTER, R. 1999. *Ostrakoden: 255 Einzeldarstellungen*. Ferdinand Enke Verlag, Stuttgart.
- HORNE, D. J., COHEN, A. and MARTENS, K. 2002. Taxonomy, morphology and biology of Quaternary and living Ostracoda. 5–36. In HOLMES, J. A. and CHIVAS, A. (eds). *The Ostracoda: Applications in Quaternary research*. Geophysical Monograph Series, **131**. American Geophysical Union.
- BRANDÃO, S. N. and SLIPPER, I. J. 2011. The Platycopid signal deciphered: responses of ostracod taxa to environmental change during the Cenomanian-Turonian Boundary Event (Late Cretaceous) in SE England. *Palaeogeography, Palaeoclimatology, Palaeoecology*, **308**, 304–312.
- ISOZAKI, Y. 1997. Permo-Triassic boundary superanoxia and stratified superocean: records from lost deep sea. *Science*, **276**, 235–238.
- JAANUSSON, V. 1985. Functional morphology of the shell in platycopid ostracodes: a study of arrested evolution. *Lethaia*, **18**, 73–84.
- JAHN, A., GAMENICK, I. and THEEDE, H. 1996. Physiological adaptations of *Cyprideis torosa* (Crustacea, Ostracoda) to hydrogen sulphide. *Marine Ecology Progress Series*, **142**, 215–223.
- JOACHIMSKI, M. M., LAI, X., SHEN, S., JIANG, H., LUO, G., CHEN, B., CHEN, J. and SUN, Y. 2012. Climate warming in the latest Permian and the Permian–Triassic mass extinction. *Geology*, **40**, 195–198.
- JONES, T. R. 1901. On some Carboniferous shale from Siberia. *Geological Magazine*, **8**, 433–436.
- KAJIYAMA, E. 1913. On the Ostracoda from Misaki. Part 3. *Doubutsugaku Zasshi*, **25**, 1–16.
- KIDDER, D. L. and WORSLEY, T. R. 2004. Causes and consequences of extreme Permo-Triassic warming to globally equable climate and relation to the Permo-Triassic extinction and recovery. *Palaeogeography, Palaeoclimatology, Palaeoecology*, **203**, 207–237.
- KIESSLING, W., SCHOBEN, M., GHADERI, A., HAIRAPETIAN, V., LEDA, L. and KORN, D. 2018. Pre-mass extinction decline of latest Permian ammonoids. *Geology*, **46**, 283–286.
- KOLLMANN, K. 1960. Ostracoden aus der alpinen Trias Österreichs. I. *Parabairdia* n. g. und *Ptychobairdia* n. g. (Bairdiidae). *Jahrbuch der Geologischen Bundesanstalt, Sonderband*, **5**, 79–105.
- KORN, D., GHADERI, A., LEDA, L., SCHOBEN, M. and ASHOURI, A. R. 2016. The ammonoids from the Late Permian *Paratiroplites* Limestone of Julfa (East Azerbaijan, Iran). *Journal of Systematic Palaeontology*, **14**, 841–890.
- KORNIKER, L. S. 1961. Ecology and taxonomy of recent Bairdiinae (Ostracoda). *Micropaleontology*, **7**, 55–70.
- KOTLYAR, G. V., ZAKHAROV, Y. D., KOCZYRKEVICZ, B. V., KROPATCHEVA, G. S., ROSTOVCEV, L. O., CHEDIJA, I. O., VUKS, G. P. and GUSEVA, E. A. 1983. *Proekt No 106 ("Permo-Triasovaya stadiya geologicheskoy evolyutsii") Mezhdunarodnoy programmy geologicheskoy korrelyatsii. Posdnepermiskiy etap evolyutsii organicheskogo mira. Dzhulfieskiy i dorashamskiy yarusy SSSR (Evolution of the latest Permian biota, Dzhulfian and Dorashamian stages of the USSR)*. Akademiya Nauk SSSR, Biologo-Pochvennyi Institut, Leningrad. [in Russian]
- KOZUR, H. W. 1985. Neue Ostracoden-Arten aus dem Oberen Mittelkarbon (Höheres Moskovian), Mittel- und Oberperm des Bükk-Gebirges (N-Ungarn). *Geologisch-Paläontologische Mitteilungen Innsbruck, Sonderband*, **2**, 1–145.
- 2005. Kozur, H. W. (2004). Pelagic uppermost Permian and the Permian–Triassic boundary conodonts of Iran. Part II: investigated sections and evaluation of the conodont faunas. *Hallesches Jahrbuch für Geowissenschaften, Reihe B, Beiheft*, **19**, 49–86.
- 2007. Biostratigraphy and event stratigraphy in Iran around the Permian–Triassic Boundary (PTB): implications for the causes of the PTB biotic crisis. *Global & Planetary Change*, **55**, 155–176.
- and METTE, W. 2006. *Iranokirkbya brandneri* n. gen. n. sp., a new kirkbyid ostracod from the Late Permian (Dorashamian) of Zal, NW Iran. *GeoAlp*, **3**, 85–91.
- KRISTAN-TOLLMANN, E. 1991. Ostracods from the Middle Triassic Sina Formation (Aghdarband Group) in NE-Iran. *Abhandlungen der Geologischen Bundesanstalt*, **38**, 195–200.
- KÜLKÖYLÜOĞLU, O. 2004. On the usage of ostracods (Crustacea) as bioindicator species in different aquatic habitats in the Bolu region, Turkey. *Ecological Indicators*, **4**, 139–147.
- MEISCH, C. and RUST, R. W. 2003. *Thermopsis thermophila* n. gen. n. sp. from hot springs in Nevada, USA (Crustacea, Ostracoda). *Hydrobiologia*, **499**, 113–123.
- LATREILLE, P. A. 1806. *Genera crustaceorum et insectorum: Secundum ordinem naturalem in familias disposita, iconibus exemplisque plurimis explicata. Tomus I. Amand Koenig, Paris*, 301 pp.
- LAU, K. V., MAHER, K., ALTINER, D., KELLEY, B. M., KUMP, L. R., LEHRMANN, D. J., SILVA-TAMAYO, J. C., WEAVER, K. L., YU, M. and PAYNE, J. L. 2016. Marine anoxia and delayed Earth system recovery after the end-Permian extinction. *Proceedings of the National Academy of Sciences*, **113**, 2360–2365.
- LEDA, L., KORN, D., GHADERI, A., HAIRAPETIAN, V., STRUCK, U. and REIMOLD, W. U. 2014. Lithostratigraphy and carbonate microfacies across the Permian–Triassic boundary near Julfa (NW Iran) and in the Baghuk Mountains (Central Iran). *Facies*, **60**, 295–325.
- LIU, H., WANG, Y., YUAN, A., YANG, H., SONG, H. and ZHANG, S. 2010. Ostracod fauna across the Permian–Triassic boundary at Chongyang, Hubei Province, and its implication for the process of the mass extinction. *Science China Earth Sciences*, **53**, 810–817.
- MADDOCKS, R. F. 1969. Revision of Recent Bairdiidae (Ostracoda). *United States National Museum Bulletin*, **295**, 1–126.
- MANDELSTAM, M. I. 1960. [Subfamily Sigilliuminae]. 398. In CHERNYSHEVA, N. E. (ed.) *Osnovy paleontologii: Arthropoda, Trilobitomorpha et Crustaceomorpha*. State Scientific Technological Publishing House, Moscow.

- MCCOY, F. 1844. *A synopsis of the characters of the Carboniferous limestone fossils of Ireland*. Dublin University Press, 207 pp.
- MELNYK, D. H. and MADDOCKS, R. F. 1988. Ostracode biostratigraphy of the Permo-Carboniferous of central and north-central Texas, Part I: paleoenvironmental framework. *Micropaleontology*, **34**, 1–20.
- MESQUITA-JOANES, F., SMITH, A. J. and VIEHBERG, F. A. 2012. The ecology of Ostracoda across levels of biological organisation from individual to ecosystem: a review of recent developments and future potential. 15–35. In HORNE, D. J., HOLMES, J., RODRIGUEZ-LAZARO, J. and VIEHBERG, F. A. (eds). *Ostracoda as proxies for Quaternary climate change*. Elsevier.
- METTE, W. 2008. Upper Permian and lowermost Triassic stratigraphy, facies and ostracods in NW Iran: implications for the P/T extinction event. *Stratigraphy*, **5**, 205–219.
- 2010. Ostracods from the Upper Permian and Permian/Triassic boundary interval of Northwest Iran. *Revista Española de Micropaleontología*, **42**, 11–35.
- MODIG, H. and ÓLAFSSON, E. 1998. Responses of Baltic benthic invertebrates to hypoxic events. *Journal of Experimental Marine Biology & Ecology*, **229**, 133–148.
- MOORE, R. C. 1961. *Treatise on invertebrate paleontology. Part Q. Arthropoda 3. Crustacea, Ostracoda*. Geological Society of America & University of Kansas Press.
- MÜLLER, G. W. 1894. Die Ostracoden des Golfes von Neapel und der angrenzenden Meeresabschnitte. *Flora & Fauna Neapel*, **21**, 1–413.
- 1906. Ostracoda. *Wissenschaftliche Ergebnisse der Deutsche Tiefsee-Expedition 1898–1899*, **8**, 154 pp.
- MUTTONI, G., GAETANI, M., KENT, D. V., SCIUNNACH, D., ANGIOLINI, L., BERRA, F., GARZANTI, E., MATTEI, M. and ZANCHI, A. 2009. Opening of the Neo-Tethys Ocean and the Pangea B to Pangea A transformation during the Permian. *GeoArabia*, **14**, 17–48.
- OZAWA, H. 2013. The history of sexual dimorphism in Ostracoda (Arthropoda, Crustacea) since the Palaeozoic. 51–80. In MORIYAMA, H. (ed.) *Sexual dimorphism*. IntechOpen, Rijeka, 149 pp.
- PAYNE, J. L., LEHRMANN, D. J., FOLLETT, D., SEIBEL, M., KUMP, L. R., RICCARDI, A., ALTINER, D., SANO, H. and WEI, J. 2007. Erosional truncation of uppermost Permian shallow-marine carbonates and implications for Permian–Triassic boundary events. *Geological Society of America Bulletin*, **119**, 771–784.
- PETERSON, R. M. and KAESLER, R. L. 1980. Distribution and diversity of ostracode assemblages from the Hamlin shale and the Americus Limestone (Permian, Wolfcampian) in Northeastern Kansas. *The University of Kansas Paleontological Contributions*, **100**, 1–26.
- RICHOZ, S., KRYSZYN, L., BAUD, A., BRANDNER, R., HORACEK, M. and MOHTAT-AGHAI, P. 2010. Permian–Triassic boundary interval in the Middle East (Iran and N. Oman): progressive environmental change from detailed carbonate carbon isotope marine curve and sedimentary evolution. *Journal of Asian Earth Sciences*, **39** (4), 236–253.
- ROSSI, V., TODESCHI, E., GANDOLFI, A., INVIDIA, M. and MENOZZI, P. 2002. Hypoxia and starvation tolerance in individuals from a riverine and a lacustrine population of *Darwinula stevensoni* (Crustacea: Ostracoda). *Archiv für Hydrobiologie*, **154**, 151–171.
- RUZHENCEV, V., SARYTCHEVA, T. and SHEVYREV, A. 1965. Biostratigraficheskie vyvody. *Trudy Paleontologicheskogo Instituta Akademii Nauk SSSR*, **108**, 93–116. [in Russian]
- SARS, G. O. 1866. Oversigt af marine Ostracoder. *Norske Videnskaps-Akademi, Förhandlingar*, **1865**, 1–130. [in Norwegian]
- 1887. Nye bidrag til kundskaben om Middelhavets invertebratfauna. IV, Ostracoda mediterranea (sydeuropæiske Ostracoder). *Archiv for Matematik og Naturvidenskab*, **12**, 173–324.
- 1922–1928. An account of the Crustacea of Norway. Vol. 9, Crustacea. *Bergen Museum*, **9**, 1–277.
- SATO, T. and KAMIYA, T. 2007. Taxonomy and geographical distribution of recent *Xestoleberis* species (Cytheroidea, Ostracoda, Crustacea) from Japan. *Paleontological Research*, **11**, 183–228.
- SCHOBLEN, M., JOACHIMSKI, M. M., KORN, D., LEDA, L. and KORTE, C. 2014. Palaeotethys seawater temperature rise and an intensified hydrological cycle following the end-Permian mass extinction. *Gondwana Research*, **26**, 675–683.
- SCOTT, H. W. 1959. The type species of *Paraparchites* Ulrich & Bassler. *Journal of Paleontology*, **33**, 670–674.
- 1961. Suborder Beyrichicopina Scott n. suborder. Suborder Kloedenellocopina Scott n. suborder. Q111–Q180. In MOORE, R. C. (ed.) *Treatise on invertebrate paleontology. Part Q. Arthropoda 3. Geological Society of America & University of Kansas Press*.
- SHEN, S.-Z. and MEI, S.-L. 2010. Lopingian (Late Permian) high resolution conodont biostratigraphy in Iran with comparison to South China zonation. *Geological Journal*, **45**, 135–161.
- SHI, C.-G. and CHEN, D.-Q. 1987. The Changhsingian ostracodes from Meishan, Changxing, Zhejiang. *Stratigraphy and Palaeontology of Systemic Boundaries in China; Permian and Triassic Boundary*, **1**, 23–80. [in Chinese with English abstract]
- 2002. Late Permian ostracodes from Heshan and Yishan of Guangxi. *Bulletin of the Nanjing Institute of Geology & Palaeontology*, **15**, 47–129.
- SLIPPER, I. J. 2005. Ostracod diversity and sea-level changes in the Late Cretaceous of southern England. *Palaeogeography, Palaeoclimatology, Palaeoecology*, **225**, 266–282.
- SMITH, R. J. and HIRUTA, S. 2004. A new species of *Metacypris* (Limnocytherinae, Cytheroidea, Ostracoda, Crustacea) from Hokkaido, Japan. *Species Diversity*, **9**, 37–46.
- and KAMIYA, T. 2002. The ontogeny of *Neonesidea oligodentata* (Bairdioidea, Ostracoda, Crustacea). *Hydrobiologia*, **489**, 245–275.
- 2005. The ontogeny of *Uncinocythere occidentalis* (Kozloff and Whitman, 1954) Hart, 1962 (Crustacea). *Hydrobiologia*, **538**, 217–229.
- SOHN, I. G. 1960. Paleozoic species of *Bairdia* and related genera. *United States Geological Survey Professional Paper*, **330-A**, 1–105.

- 1970. Early Triassic marine ostracods from the Salt Range and Surghar Range, West Pakistan. 193–206. In KUMMEL, B. and TEICHERT, C. (eds). *Stratigraphic boundary problems: Permian and Triassic of West Pakistan*. University of Kansas Special Publication, 4.
- SONG, H., WIGNALL, P. B., TONG, J., BOND, D. P., SONG, H., LAI, X., ZHANG, K., WANG, H. and CHEN, Y. 2012. Geochemical evidence from bio-apatite for multiple oceanic anoxic events during Permian–Triassic transition and the link with end-Permian extinction and recovery. *Earth & Planetary Science Letters*, **353**, 12–21.
- — CHU, D., TONG, J., SUN, Y., SONG, H., HE, W. and TIAN, L. 2014. Anoxia/high temperature double whammy during the Permian–Triassic marine crisis and its aftermath. *Scientific Reports*, **4**, 4132.
- STAMPFLI, G. M. and BOREL, G. 2002. A plate tectonic model for the Paleozoic and Mesozoic constrained by dynamic plate boundaries and restored synthetic oceanic isochrons. *Earth & Planetary Science Letters*, **196**, 17–33.
- STEPANOV, D. L., GOLSHANI, F. and STÖCKLIN, J. 1969. Upper Permian and Permian–Triassic Boundary in North Iran. *Geological Survey of Iran, Report*, **12**, 1–72.
- SUN, Y., JOACHIMSKI, M. M., WIGNALL, P. B., YAN, C., CHEN, Y., JIANG, H., WANG, L. and LAI, X. 2012. Lethally hot temperatures during the Early Triassic greenhouse. *Science*, **338**, 366–370.
- SVENSEN, H., PLANKE, S., POLOZOV, A. G., SCHMIDBAUER, N., CORFU, F., PODLADCHIKOV, Y. Y. and JAMTVEIT, B. 2009. Siberian gas venting and the end-Permian environmental crisis. *Earth & Planetary Science Letters*, **277**, 490–500.
- SWARTZ, F. M. 1936. Revision of the Primitiidae and Beyrichidae with new Ostracoda from the Lower Devonian of Pennsylvania. *Journal of Paleontology*, **10**, 541–586.
- SYLVESTER-BRADLEY, P. C. 1961. Suborder Metacopina Sylverter-Bradley, n. suborder. Q358–Q359. In MOORE, R. C. (ed.) *Treatise on invertebrate paleontology. Part Q. Arthropoda 3. Crustacea, Ostracoda. Crustacea, Ostracoda*. Geological Society of America & University of Kansas Press.
- TANAKA, G. and IKEYA, N. 2002. Migration and speciation of the *Loxocochoa japonica* species group (Ostracoda) in East Asia. *Paleontological Research*, **6**, 265–284.
- and SETO, K. 2010. Description of appendages from three marine trachyleberidid species (Ostracoda, Crustacea) from Japan. *Journal of Micropaleontology*, **29**, 5–16.
- TÓTH, E. and CSÉFÁN, T. 2018. Rare myodocopid ostracods from Mesozoic sections of Hungary: summary, revision and description of new taxa. *Zootaxa*, **4374**, 350–374.
- ULRICH, E. O. 1891. New and little known American Paleozoic Ostracoda. Pt. 3, Carboniferous species. *Cincinnati Society of Natural History Journal*, **13**, 200–211.
- and BASSLER, R. S. 1906. New American Paleozoic Ostracoda. Notes and descriptions of Upper Carboniferous genera and species. *Proceedings of the United States National Museum*, **30**, 149–164.
- — 1908. New American Paleozoic Ostracoda. Preliminary revision of the Beyrichiidae, with descriptions of new genera. *Proceedings of the United States National Museum*, **35**, 277–340.
- — 1923. Paleozoic Ostracoda: their morphology, classification, and occurrence. *Maryland Geological Survey, Silurian*, **9**, 271–391.
- VANDEKERKHOVE, J., MARTENS, K., ROSSETTI, G., MESQUITA-JOANES, F. and NAMOTKO, T. 2013. Extreme tolerance to environmental stress of sexual and parthenogenetic resting eggs of *Eucypris virens* (Crustacea, Ostracoda). *Freshwater Biology*, **58**, 237–247.
- WAN, J., YUAN, A., CRASQUIN, S., JIANG, H., YANG, H. and HU, X. 2019. High-resolution variation in ostracod assemblages from microbialites near the Permian–Triassic boundary at Zuodeng, Guangxi region, South China. *Palaeogeography, Palaeoclimatology, Palaeoecology*, **535**, 109349.
- WANG, S.-Q. 1978. Late Permian and Early Triassic ostracods of western Guizhou and northeastern Yunnan. *Acta Palaeontologica Sinica*, **17**, 277–312.
- WICKSTROM, C. E. and CASTENHOLZ, R. W. 1973. Thermophilic ostracod: aquatic metazoan with the highest known temperature tolerance. *Science*, **181**, 1063–1064.
- — 1985. Dynamics of cyanobacterial and ostracod interactions in an Oregon hot spring. *Ecology*, **66**, 1024–1041.
- WIGNALL, P. B. and TWITCHETT, R. J. 1996. Oceanic anoxia and the end Permian mass extinction. *Science*, **272**, 1155–1158.
- YASUHARA, M., YAMAZAKI, H., IRIZUKI, T. and YOSHIKAWA, S. 2003. Temporal changes of ostracode assemblages and anthropogenic pollution during the last 100 years, in sediment cores from Hiroshima Bay, Japan. *The Holocene*, **13**, 527–536.
- ZAKHAROV, Y. D. 1992. The Permo-Triassic boundary in the southern and eastern USSR and its intercontinental correlation. 46–55. In SWEET, W. C., ZUNYI, Y., DICKINS, J. M. and HONGFU, Y. (eds). *Stratigraphy, classification and relations with the western Tethys*. World & Regional Geology, 2. Cambridge University Press.
- ZAZZALI, S., CRASQUIN, S., DECONINCK, J.-F. and FENG, Q. 2015. Biodiversity across the Guadalupian-Lopingian Boundary: first results on the ostracod (Crustacea) fauna, Chaotian section (Sichuan Province, South China). *Geodiversitas*, **37**, 283–314.
- ZHANG, F., ROMANIELLO, S. J., ALGEO, T. J., LAU, K. V., CLAPHAM, M. E., RICHOSZ, S., HERRMANN, A. D., SMITH, H., HORACEK, M. and ANBAR, A. D. 2018. Multiple episodes of extensive marine anoxia linked to global warming and continental weathering following the latest Permian mass extinction. *Science Advances*, **4**, e1602921.
- ZHENG, S. 1976. Early Mesozoic ostracods from some localities in South West China. *Acta Palaeontologica Sinica*, **15**, 77–93.